

EXPLORING POST-WILDFIRE WATER QUALITY:
THE PHOTODEGRADATION OF DISSOLVED PYROGENIC CARBON

by

JESSICA KELLY EGAN

B.S., Florida International University, 2014

A thesis submitted to the
Faculty of the Graduate School of the
University of Colorado in partial fulfillment
of the requirement for the degree of
Master of Science
Environmental Studies
2020

Committee Members:

Dr. Diane M. McKnight

Dr. Michael SanClements

Dr. Lisa Dilling

ABSTRACT

Egan, Jessica Kelly (M.S., Environmental Studies)

Exploring Post-Wildfire Water Quality: the Photodegradation of Dissolved Pyrogenic Carbon

Thesis directed by Professor Diane M. McKnight

Nearly 80% of the United States' freshwater originates in forested landscapes at risk of wildfires, which influence both the terrestrial landscape and hydrologic regime by introducing a heterogeneous spectrum of thermally altered carbon compounds, known as pyrogenic carbon (PyC). Given the projected increase in both wildfire frequency and intensity, understanding the coupling of hydrologic transport and chemical fractionation that wildfires impose on water sources is critical. New research has begun to show that PyC can be quite mobile and reactive with turnover time of decades or years in soils rather than previously assumed millennia timescales, emphasizing the importance of dissolved PyC (DPyC) translocation from soils to rivers. While riverine PyC transport has been identified as a key component of the global PyC cycle, the extent to which photodegradation contributes to both short-term and long-term DPyC chemical fraction has yet to be resolved. We investigate the role of photodegradation as a major driver altering aquatic DPyC physical and chemical properties using fluorescence spectroscopy. Artificial PyC was created by burning organic matter at various temperatures to isolate distinct portions of the PyC spectrum. The organic matter, comprised of leaves and soils, was collected from Great Smoky Mountain National Park where ongoing research was being conducted following the 2016 Chimney Tops 2

wildfire. Each temperature range of the PyC spectrum was separately leached, filtered, and the dissolved fraction was placed outside and exposed to natural sunlight for various exposure times ranging from zero to 28 days. This photodegradation experiment took place in Boulder, Colorado during the summer months to maximize daily sun exposure. Photochemistry was confirmed by monitoring the photochemical formation of hydrogen peroxide via fluorescence spectroscopy. The dissolved organic matter was characterized using ultraviolet-visible (UV-vis) absorption and excitation-emission matrix (EEM) fluorescence spectroscopy. By isolating distinct portions of the PyC spectrum, we will better be able to anticipate the fate of PyC in watersheds effected by wildfires.

DEDICATION

To Brian – thank you for joining me on this Colorado adventure and for your continuous support and love throughout this entire process. Especially for making me laugh and for always keeping me well fed. Now on to the next chapter!

To my friends and family – thank you for constantly lifting me up and making me loved and empowered. I could not have made it through this process without your unwavering support.

ACKNOWLEDGEMENTS

Thank you to several members from INSTAAR and both the McKnight and Hinckley lab groups for your time and resources in helping pull off this experiment. A special thank you to my lab assistant, Abbey Turner, for all your hard work. An extra acknowledgement to Wendy Roth for both laboratory assistance and for your willingness to always listen, care, and help.

Thank you to my parents, Bill and Michele Egan, for your endless love and support. To my dad, Bill, thank you for volunteering as both a field assistant and lab assistant – your company was much appreciated and your help was essential to the success of this research. To my mom, Michele, thank you for always demonstrating how to be an intelligent, witty, and respected woman.

Thank you to numerous friends and colleagues who emotionally carried me through this journey. A special thank you to Maggie Bowman for all your mentorship, training, friendship, and numerous happy hours – I could not have gotten through this without you. Special thank you to both Olivia Pearman and Sean Ryan for countless hours of therapeutic workouts and venting sessions – your friendships have made me a better human being and scientist.

To my advisor, Diane McKnight, thank you for advocating for me and bringing consistent enthusiasm and support to my ideas and research. It has been an honor to work alongside such a brilliant and strong female scientist. Thank you to the rest of my committee, Mike SanClements and Lisa Dilling, for your support and aid in pushing me through the finish line with this research.

Thank you to the Environmental Studies (ENVS) Program for financially supporting a portion of my research. It has been an honor to be a part of the ENVS family and to stand alongside the numerous brilliant, thoughtful, and passionate students and researchers within this program.

Thank you to the National Ecological Observatory Network for financially supporting the Great Smoky Mountain National Park research, travel, and collaboration.

Thank you to the Atmospheric and Oceanic Sciences Department for accommodating access to the Skywatch Observatory for the duration of the experiment and for numerous teaching assistant appointments.

TABLE OF CONTENTS

INTRODUCTION	1
BACKGROUND	1
Pyrogenic Carbon.....	1
Photodegradation	5
Analyses.....	7
i. Photochemical analysis.....	8
ii. Excitation-Emission Matrices (EEMs).....	9
iii. Parallel factor analysis (PARAFAC).....	14
METHODS	15
Field site and sample collection.....	15
Burning	16
Leaching.....	18
Photodegradation – incubation period	20
Analyses.....	23
i. Photochemical analysis.....	23
ii. Excitation-Emission Matrices (EEMs).....	25
RESULTS AND DISCUSSION.....	26
Quantifying solar radiation	26
UV ₂₅₄ absorption.....	28
Hydrogen peroxide: a confirmation of photolysis	30
Fluorescence Spectroscopy	34
i. Excitation-emission matrices	34
ii. pH effects.....	38
iii. Fluorescence indices.....	40
iv. PARAFAC: Component Loading.....	48
SUMMARY	60
REFERENCES	65
LIST OF ACRONYMS	74

LIST OF TABLES

Table 1: Fluorescence Indices.....	11
Table 2: Sample matrix of burn treatment and solar radiation exposure	20
Table 3: Hydrogen Peroxide Reagent Composition	24
Table 4: Cumulative Solar Radiation.....	27
Table 5 Summary of fluorescence indices and PARAFAC components for Day 14	41
Table 6: Percent change of fluorescence indices	42
Table 7: Max emission signal at EX ₃₇₀ comparison on day 0 and 25.....	45
Table 8: Percent change of absolute loadings (Day 0 to 25)	48
Table 9: Model fit parameters for all Light-exposed samples	50
Table 10: Summary values and trends of photodegraded DPyOM compared to photodegraded NOM	62

LIST OF FIGURES

Figure 1: Chemical compounds and transformations associated with increased thermal alteration. Figure adapted from Lauren Matosziuk, Oregon State University.....	2
Figure 2: Fate and transport of dissolved black carbon (DBC), which is comparable to DPyC. from terrestrial to marine systems (Image from Masiello and Louchouart 2013).....	3
Figure 3: The reduction (left to right) and oxidation (right to left) pathways between oxidized quinones (A and D), semiquinones (B and E), and reduced hydroquinones (C and F). A-C represents reduction of benzoquinone. D-F represent reduction pathway of naphthoquinone. Figure borrowed from Cory and McKnight 2005.	13
Figure 4: Batch leaching of the separate burn treatments. From left to right: solution blank, outside burn, 700, 550, 400, 300, 200°C, and unburned. The burned OM is leaching in a solution of sodium bicarbonate and formaldehyde.....	18
Figure 5: Light-exposed leachates were placed on wire racks within the Skywatch Observatory. Samples were opened and turned daily. The leachates were placed in the same order on each rack in triplicate groups. The left most rack, starting from top to bottom and left to right, the leachates appear as: solution blank, 200°C, unburned, 300°C, outside, 400, 550, and 700°C.	21
Figure 6: Figure adapted from Kok et al. Oxidation of pHPAA by H ₂ O ₂ and peroxidase into the fluorescent pHPAA dimer (Kok et al. 1986; Schylte-Ladbeck et al. 2003)	23
Figure 7: Daily solar radiation throughout the duration of the photoexposure experiment. Missing UVA data on July 31 st	27
Figure 8: UV absorbance throughout 25-day experiment.....	29
Figure 9: Hydrogen Peroxide concentrations compare to UV absorbance throughout the duration of the experiment.	30
Figure 10: Hydrogen peroxide concentrations over time.....	32
Figure 11: Ratio of hydrogen peroxide concentration to UV absorbance over time	33
Figure 12: Excitation-emission matrix comparison across burn treatments and light-exposed versus dark-control groups.....	37
Figure 13: pH of the various treatments and groups throughout the 25-day experiment.	38

Figure 14: Fluorescence indices over time. All axes scales are the same except for the HIX and FI maximums for the 700°C treatment. Each column represents various burn treatments and each row represents a fluorescence index. The humification index (HIX) is the first row (14-a), freshness index is the second row (14-b), fluorescence index (FI) is the third row (14-c), Maximum emission at 370nm is the fourth row (14-d), and redox index (RI) is the fifth row (14-e). 40

Figure 15: Absolute loading and percent loading of oxidized quinone-like (Q1, Q2, and Q3) components. 52

Figure 16: Absolute loading and percent loading of reduced quinone-like components, including semiquinone-like (SQ1, SQ2, and SQ3) and hydroquinone-like (HQ) component 55

Figure 17: Absolute loading and percent loading of protein, amino acid-like components (tryptophan and tyrosine) and combined percent loadings of both tryptophan and tyrosine (Protein) 58

INTRODUCTION

Nearly 80% of the United States' freshwater originates in forested landscapes at risk of wildfires (United States Geological Survey 2016), which influence both the terrestrial landscape and hydrologic regime by introducing a heterogeneous spectrum of thermally altered carbon compounds, known as pyrogenic carbon (PyC) (Bird et al. 2015). Globally, landscape fires burn 3-5million km² of Earth's surface annually (Jones et al. 2019). Given the projected increase in both wildfire frequency and intensity, understanding the coupling of hydrologic transport and chemical fractionation that wildfires impose on water sources is critical (Myers-Pigg et al. 2017; Soong et al. 2015).

BACKGROUND

Pyrogenic Carbon

Pyrogenic carbon (PyC) results from the incomplete combustion of biomass or fossil fuel (Bird et al. 2015). The formation temperature and parent organic material largely determine the molecular structure of PyC. Figure 1 illustrates the typical chemicals and transformations that accompany increased thermal alteration. The PyC spectrum is dictated primarily by formation temperature, where lower temperatures produce low molecular weight organic acids (LMWOA), that are typically viewed as labile and reactive. These compounds include thermal degradation byproducts of cellulose, have increased oxygenated functional groups, and are a source of highly mobile soil carbon. As formation temperature increases, there is a reduction in oxygenated functional groups

and an increase in C:N, C:O, and C:H ratios, resulting in an increase in high molecular weight (HMW) aromatic and condensed aromatic compounds – including polycyclic aromatic hydrocarbons (PAHs). Increasing aromaticity is typically associated with increased hydrophobicity, recalcitrance, and decreased reactivity.

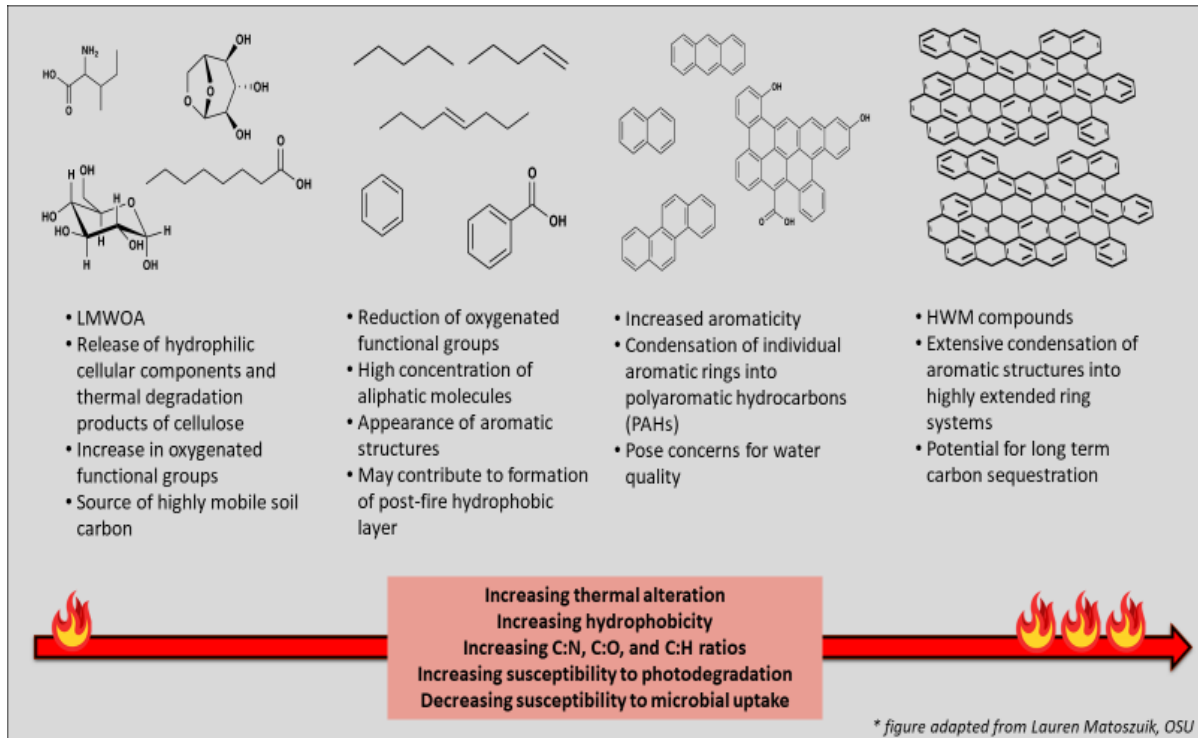


Figure 1: Chemical compounds and transformations associated with increased thermal alteration. Figure adapted from Lauren Matosziuk, Oregon State University.

Many forested areas at risk of wildfire contain headwater streams that contribute to the production, transport, and quality of dissolved organic carbon (DOC) (Bird et al. 2015). DOC is a major carbon flux to oceans and chemical analyses show that up to 10% of global DOC appears as DPyC (Myers-Pigg et al. 2017; Wagner 2015) – indicating DPyC is an important component to consider in the global carbon cycle (figure 2). Oceans are the largest global PyC sink, further

emphasizing that reactive riverine transport is a critical area of DPyC (Bird et al. 2015). Research has increasingly highlighted the gaps in PyC production and storage – emphasizing that degradation and transport mechanisms need to be further investigated. Estimated PyC production rates of 50-300 Tg/yr, including both natural and anthropogenic sources, would over calculate the amount of PyC in soil C to be between 25-125% (Bostick et al. 2018; Jones et al. 2019; Forbes et

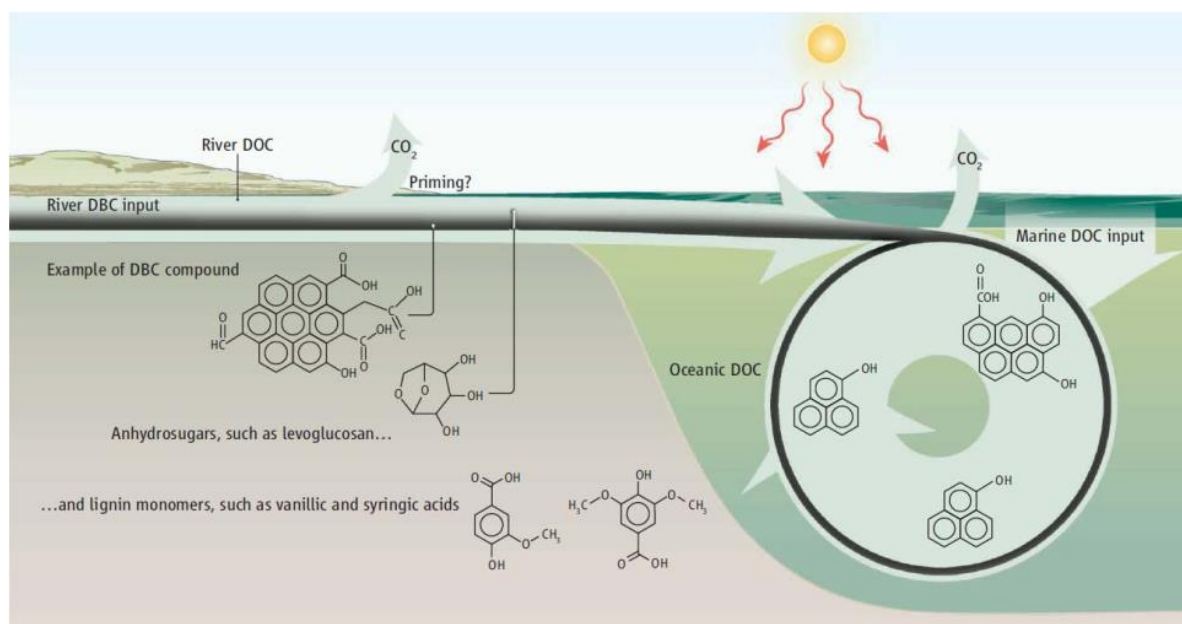


Figure 2: Fate and transport of dissolved black carbon (DBC), which is comparable to DPyC, from terrestrial to marine systems (Image from Masiello and Louchouart 2013).

al. 2006; Masiello 2004). PyC typically comprises 14% of soil C, 10% of riverine DOC, 16% of riverine particulate OC (POC), and 10-30% of the organic C fraction in oceanic sediments (Jones et al. 2019; Reisser et al. 2016; Jaffe et al. 2013; Coppola et al. 2018; Bird et al. 2015; Masiello and Druffel 1998).

PyC is ubiquitous throughout the environment yet the role of PyC in the global carbon cycle remains poorly understood (Bostick et al. 2018; Bird et al. 2015). Most PyC is deposited on

the terrestrial landscape in the particulate form (PPyC). PyC degradation can occur by various processes: photodegradation, erosion, mineralization, sorption, oxidation, and microbial respiration (Bird et al. 2015; Cotrufo et al. 2016). PPyC can be transported horizontally by wind and water or can be stabilized within soils. However, an imbalance exists between PyC production and loss, which cannot be explained by transference within the soil profile (Wagner 2015; Masiello 2004). It has been estimated that only 17% of PyC is transferred vertically into the soil, where HMW compounds sorb to minerals that can potentially offer a steady source of DPyC on longer timescales (Wagner 2015). These condensed, HMW compounds are typically characterized using benzene polycarboxylic acids (BPCA) markers, where the more carboxylic acid substitutions (represented by B6CA or B5CA markers) indicate more condensed parent molecules (Dittmar 2008; Wagner 2015).

More recent research shows that PyC can be quite mobile and reactive with turnover times in soils being decades or years, rather than previously assumed millennia timescales, indicating the importance of DPyC translocation from soils to rivers (Bird et al. 2015; Dittmar et al. 2012; Wagner 2015). Hydrologic transport removes a significant portion of PyC from the terrestrial landscape and soil profile. Overland flow removes surface PyC – potentially contributing more condensed DPyC forms (enriched with B6CA/B5CA markers) on shorter timescales; whereas groundwater and baseflow contributes less condensed DPyC forms (containing more B4CA/B3CA markers) (Wagner 2015). This same research found that the HMW DPyC was more photolabile compared to the LMW DPyC. While investigating DPyC photodegradation within the ocean, the largest DPyC sink, Stubbins et al. (2012) hypothesizes that DPyC survival depends more so on

exposure (or lack of exposure) to photodegradation byway of cycling, rather than PyC's assumed inertness. Understanding PyC degradation mechanisms and pathways is critical in determining PyC transport between source (wildfire production), intermediate zones (soils, streams, and atmosphere), and sink (ocean sediments) (Bird et al. 2015).

Photodegradation

Photolysis of DOM is an important process of nutrient cycling and transport. Photochemical reactions take place when a compound acts as a light absorbing molecule (chromophore). The extent of photodegradation is dictated by a compounds molecular structure, size, and substrate color, as well as ambient conditions of oxygen availability, depth of light penetration, and temperature (McKnight and Duren 2004). The role of chromophoric DOM (CDOM) plays an important role in the transmission or attenuation of radiation throughout the water column (Hader et al. 2003). DOM photochemical reactions can lead to both photodegradation and photoproducts. Photodegraded products generally have higher O:C and lower H:C ratios, whereas photoproducts generally have lower O:C and higher H:C ratios (Ward and Cory 2016).

Certain components of DOM are more susceptible to the absorption of solar radiation. Three major DOM groups to consider are aromatic carbon, carboxyl carbon, and phenolic carbon (Ward and Cory 2016). The aromatic-C group serves as the main light absorbing fraction that initiates and assists in both direct and indirect photochemical reactions. DOM photolysis involving the aromatic-C group contributes to the production of reactive radicals or intermediate species, partially oxidized compounds (LMW, aliphatic compounds), or complete photooxidation to CO₂

(Ward and Cory 2016). The carboxyl-C group is the portion of DOM that is most susceptible to complete photooxidation to CO₂ but can also produce less reactive functional groups, like esters (Ward and Cory 2016). The phenolic-C group acts as an antioxidant by suppressing degradation through quenching of indirect reactions involving reactive oxygen species (Ward and Cory 2016).

About 80% of DOM from freshwater systems is comprised of phenolic and other aromatic humic compounds, known as fulvic and humic acids (Hader et al. 2003). These humic substances are a key factor in DOM absorption of radiation (Hader et al. 2003). Fulvic acids are soluble, hydrophilic, LMW, and contain various functional groups (including carboxylic acids), whereas humic acids are less soluble and HMW (Hader et al. 2003). Fulvic acids originate from either allochthonous (decomposed plant or soil) sources or autochthonous (produced by algae and bacteria) sources (McKnight and Aiken 1998; Cory et al. 2007). When exposed to photodegrading conditions, aromatic-C moieties within fulvic acids are responsible for the loss of DOM absorbance and fluorescence (Cory et al. 2007). HMW, straight chain hydrocarbons absorb UV light less efficiently and are therefore less likely to photodissociate unless aided by sorption to a molecule or substrate that serves as the chromophore (Abrajano et al. 2007). PAHs can be susceptible to photochemical reactions and transformations under atmospheric conditions or within the photic zone the water column (Abrajano et al. 2007).

Incoming solar radiation includes radiation within the visible, ultraviolet (UV), and infrared (IR) spectrums. UV radiation is comprised of UVA (315-400nm), UVB (280-315nm), and UVC (200-280nm) (Hader et al. 2003). The earth's atmosphere filters out all UVC, so the incoming

UV radiation that reaches earth's surface is 95% UVA with the remaining 5% being UVB (World Health Organization 2016). While most UVB is filtered by the atmosphere, UVB is highly energetic and a key photoactivating agent in natural waters (World Health Organization 2016; Hader et al. 2003). UVB and UVA are the dominant radiative forces in the photochemical oxidation of DOM, but photosynthetically active radiation (PAR, 400-700nm) also plays a role (Hader et al. 2003). PAR is energetically weaker but has a deeper penetration depth into the water column (Hader et al. 2003). When quantifying the photolysis on DOM, UVB accounts for 25%, UVA for 50%, and PAR for 25% (Hader et al. 2003). A composite of 200 separate photolytic experiments, indicate that UVB is the most important portion in the photodegradation of DOM to CO₂ (Hader et al. 2003). Continued stratospheric damage with reduction of ozone could result in increased UVB penetration which would intensify photooxidation of DOM to CO₂ and accelerate biogeochemical cycling of nutrients (Hader et al. 2003).

Photodegradation of CDOM can result in more bioavailable DOM for microbes (Hader et al. 2003). DOM has components that are chemically recalcitrant, which are important in maintaining energy balance (or metabolic stability) in the system (Hader et al. 2003). Photolysis can accelerate this process causing an imbalance. Complete photooxidation of DOM to CO₂ can also occur, creating implications for climate change.

Analyses

UV-vis absorption and fluorescence spectroscopy are effective analytical techniques that aid in the characterization of DOM composition. When conducting fluorescence analysis, it is important to

adjust the absorbance of samples to below 0.2 in order to prevent inner-filter effects. Inner-filter effects are associated with the attenuation of light which influence the fluorescence signal detected by the fluorometer (Coble et al. 2014; Cory et al. 2010). The primary inner-filter effect occurs when excitation light is absorbed prior to interacting with the fluorescent molecule (Coble et al. 2014). The secondary inner-filter effect occurs when light emitted by the fluorescent molecule is absorbed prior to being detected by the instrument (Coble et al. 2014).

Fluorescence spectroscopy has proven to be a robust tool when characterizing DOM and examining photochemical changes (Coble et al. 2014; Fellman et al. 2010; Cory et al. 2007; Cory and McKnight 2005). The molecular composition and geometry of a compound determines how that compound will absorb and emit light. Fluorescence spectroscopy takes advantage of unique absorption and emission properties of a molecule. Fluorescence occurs after a molecule absorbs light in order to reach an excited state, when the molecule is in the lowest vibrational energy level of this excited state it can emit a photon in order to return to a lower energy state (Coble et al. 2014). Fluorescence is a measure of this emitted photon (Coble et al. 2014).

i. Photochemical analysis

DOM photochemical reactions can lead to both photodegraded and photoproducts. Hydrogen peroxide (H_2O_2) is a photochemical byproduct of DOM photolysis (McKay and Rosario-Ortiz 2015; Scott et al. 2003; Cooper et al. 1988). This process is illustrated by the two-step reaction (1) and (2) involving DOM, UV light, and oxygen where a superoxide radical (O_2^-) is formed first and then undergoes dismutation to form H_2O_2 (Scott et al. 2003).



The superoxide can form from a variety of pathways: photoionization of a light-absorbing substance (DOM) which generates free electrons; reduction of oxygen via an energy transfer from the excited state; electron transfer from reduced metals; or additional photocatalyzed reactions (Cooper et al. 1988). The interaction of DOM, oxygen, and UV-light can result in the formation of various reduced reactive oxygen species, one of which includes H_2O_2 (Hader et al. 2003; McKay and Rosario-Ortiz 2005). H_2O_2 does not accumulate, instead H_2O_2 is a reactive species that is available to react with other DOM constituents. The formation of H_2O_2 can significantly impact redox cycling of metals (Hader et al. 2003). In addition to H_2O_2 , DOM photolysis reactions can result in the formation of various reactive intermediate species and radicals (singlet oxygen or hydroxyl radical) that can indirectly aid in the degradation of DOM (Ward and Cory 2016).

The rate at which H_2O_2 forms depends on the concentration of a chromophore (light-absorbing substance) in natural waters (Cooper et al. 1988). H_2O_2 formation and destruction is correlated with concentrations of humic substances (Cooper et al. 1988). Lower concentrations of DOM will limit the production of the superoxide radical and H_2O_2 (McKnight and Duren 2004), so we would expect that longer UV exposure times will result in both a decrease in DOM and H_2O_2 concentrations.

ii. Excitation-Emission Matrices (EEMs)

Excitation-emission matrices (EEMs) are 3D scans representing a range of fluorescence emission signals when excited at various fixed wavelengths. EEMs provide a visual representation of

electronic transitions which render structural information regarding the DOM composition (Coble et al. 2014). Fluorescence indices are used to consolidate information contained within EEMs by using numerical values that represent a ratio of fluorescence intensity signals comparing various regions or points within the EEM (Coble et al. 2014). These indices provide information about the origin and transformation of DOM and are further explained in Table 1.

Table 1: Fluorescence Indices

Index	Parameters	Application and typical values for natural waters
Humification Index (HIX)	$\frac{EM_{435-480}}{EM_{300-345}} @ EX_{254}$	Indicates degree of humification (or maturation) <ul style="list-style-type: none"> • Lower values: decreased humification and aromaticity, potential increase in O-containing functional groups • Higher values: greater humification and aromaticity (ring structure), lower H:C, shifting to longer emission wavelengths • Typical values can vary between 0-30
Freshness Index ($\beta:\alpha$)	$\frac{EM_{380}}{EM_{420-435}} @ EX_{310}$	Indicates the proportion of the DOM that is recently produced (β peak, microbial or protein-like) or older (α peak, terrestrial or humic-like). <ul style="list-style-type: none"> • Lower values: older, more decomposed, or humic OM • Higher values: higher proportion of recently created or microbial OM • Typical value range: 0.4-1
Fluorescence Index (FI)	$\frac{EM_{470}}{EM_{520}} @ EX_{370}$	Reflects relative humic precursor material to DOM (terrestrial or microbial sources) <ul style="list-style-type: none"> • Lower values (<1.4): terrestrial sources (allochthonous or degraded plant and soil OM) • Higher values (<1.8): microbial sources (autochthonous or extracellular release and leachate from bacteria and algae) • Typically range for natural waters: 1.2-1.8
Redox Index (RI)	$\frac{Q_{red}}{Q_{red} + Q_{ox}}$	Measure of the redox state of quinone-like moieties in humic DOM. Based on Cory-McKnight PARAFAC components. <ul style="list-style-type: none"> • Low values (<0.4): quinone-like components more oxidized; blue-shifted • High values (>0.5): quinone-like components more reduced; red-shifted • Typical values: ~0.42

sources: Coble et al. 2014; McKnight et al. 2001; Cory et al. 2007; Hansen et al. 2016; Miller et al. 2006; Macalady and Walton-Day 2009

a. Humification Index (HIX)

The humification index (HIX) represents a ratio of emission signals at excitation 254nm, where the sum of emission signals from 435-480nm is divided by the sum of emission signals from 330-345nm (Coble et al. 2014). HIX provides information on the degree of humification (or maturation) of DOM, meaning higher HIX values are generally representative of higher aromaticity and reflective of longer soil maturation involving more biogeochemical cycling or processing. Higher HIX values are often associated with red-shifted DOM, meaning that an increase in C:H ratios resulted in shifting to lower energy, higher emission wavelengths.

b. Freshness Index ($\beta:\alpha$)

The freshness index ($\beta:\alpha$) represents the ratio of emission signals at excitation 310nm, where emission at 380nm is divided by the maximum emission intensity with the range of emission signals 420-435nm (Coble et al. 2014; Hansen et al. 2016). The β peak represents more recently created OM (ie. microbial) and the α peak corresponds to older or more decomposed OM (ie. humic). This index indicates the proportion of recently produced DOM, where higher values correspond to more recently produced (or ‘fresher’) DOM.

c. Fluorescence index (FI)

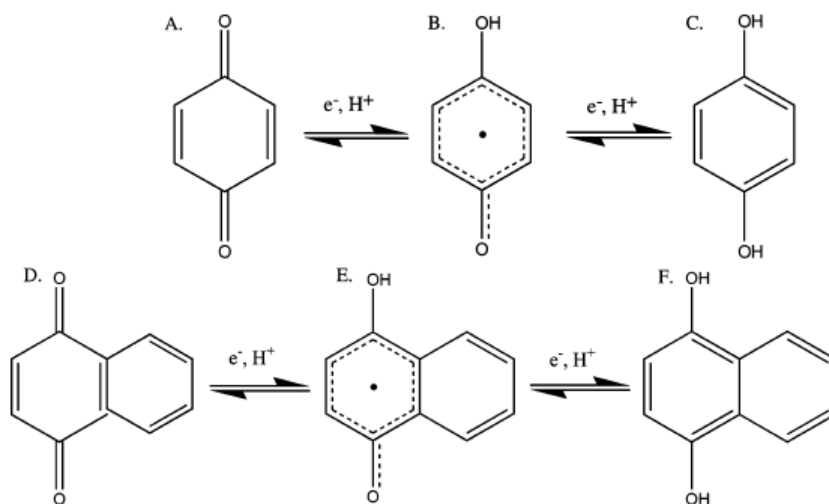
The fluorescence index (FI) measures the ratio of emission intensities 470nm to 520nm, at an excitation of 370nm (Coble et al. 2014). The FI index is commonly used to indicate whether the precursor material is terrestrial or microbial, where lower values (near 1.3) are indicative of

terrestrial origin and higher values (near 1.8) are indicative of microbial origin or influence. However, an increase in FI can correspond to a shift of the main peak to lower emission wavelengths (Cory and McKnight 2005; Coble et al. 2014).

d. Redox Index (RI)

Spectral shifts have been observed with DOM changes in redox state (Cory and McKnight 2005; Miller et al. 2006). The redox index (RI) is a measure of the redox state of quinone-like moieties in humic DOM (Miller et al. 2006; Coble et al. 2014). An example of these pathways can be seen in Figure 3.

This index provides information about humic substances role in electron shuttling (Cory and McKnight 2005; Coble et al. 2014).



RI is based on components derived from the Cory-McKnight

Figure 3: The reduction (left to right) and oxidation (right to left) pathways between oxidized quinones (A and D), semiquinones (B and E), and reduced hydroquinones (C and F). A-C represents reduction of benzoquinone. D-F represent reduction pathway of naphthoquinone. Figure borrowed from Cory and McKnight 2005.

PARAFAC model (2005), which is explained in the following section. RI measures the sum of reduced quinone-like inputs over total quinone-like inputs, $RI = \frac{Q_{red}}{Q_{red} + Q_{ox}}$. Where Q_{red} represents the sum of the reduced quinone-like components: SQ1, SQ2, SQ3, and HQ, and Q_{ox} represents the

sum of the oxidized quinone-like components, Q1, Q2, Q3. Lower RI values (less than 0.4 or closer to zero) indicate that the quinone-like components are more oxidized, whereas higher RI values (greater than 0.5 or closer to 1) indicate that the quinone-like components are more reduced.

iii. Parallel factor analysis (PARAFAC)

Parallel factor analysis (PARAFAC) is a statistical method for analyzing EEMs using signal peak components that correspond to various classes of fluorophores (Cory et al. 2007; Coble et al. 2014; Miller et al. 2006). The PARAFAC approach reveals the most influential fluorescing components without making assumptions about the curve shapes. The Cory and McKnight (2005) PARAFAC model identifies 13 fluorescing components influencing the appearance of EEMs. Some of these components reflect information about known classes of compounds, including quinones and amino acids.

It has been demonstrated fluorescence spectra of quinone shifts reveal a change in redox state (Cory and McKnight 2005; Miller et al. 2006). Quinones are a key class of molecules involved in DOM redox reactions and the varying fluorescent capabilities make quinones useful in detecting photochemical reactions (Cory and McKnight 2005; Poulson and Birks 1989; Coble et al. 2014). Quinones can exist in three redox states: (1) quinones, which are oxidized and poor fluorophores, (2) semiquinones, which are reduced radicals, and (3) hydroquinones, which are reduced and highly fluorescent (Cory and McKnight 2005; Coble et al. 2014). Seven components within the Cory and McKnight PARAFAC model include quinone-like components. PARAFAC components C11, C2, and C12 respectively correspond to quinone-like moieties labeled Q1, Q2,

and Q3. PARAFAC components C5, C7, and C9 respectively correspond to semiquinone-like moieties labeled SQ1, SQ2, and SQ3. PARAFAC component C4 corresponds to hydroquinone-like moiety. PARAFAC components C8 and C13 respectively correspond to amino acid-like, protein moieties tryptophan and tyrosine. The remaining four components, C1, C3, C6, and C10, have unknown molecular associations (Cory and McKnight 2005; Cory et al. 2005).

METHODS

Field site and sample collection

All samples were collected from unburned areas within and around Great Smoky Mountain National Park (GRSMNP), Tennessee as part of an NSF RAPID grant and in partnership with the National Ecological Observatory Network (NEON). Samples were gathered from both within and outside the park boundaries in order to minimize disruption to the GRSMNP system. Within GRSMNP samples were collected near Briar Branch, Bearwallow, and the Twin Creeks Science Center. Outside of the park, samples were collected near a residential area in Sevierville, TN. GRSMNP is in eastern Tennessee within the southern Appalachian Mountains. GRSMNP is a densely vegetated area with extensive leaf litter. The sample locations are primarily characterized as submesic to mesic oak-hardwood forests, southern Appalachian cove hardwood, and montane alluvial forest (Matosziuk et al. 2020). Primary tree species include hickory (*Carya* sp.), oak (*Quercus* sp.), red maple (*Acer rubrum*), eastern white pine (*Pinus strobus* L.), American Beech (*Fagus grandifolia*), sassafras (*Sassafras albidum*), and black gum (*Nyssa sylvatica*). Additional plant species include Virginia creeper (*Parthenocissus quinquefolia*), mountain laurel (*Kalmia*

latifolia L.), rhododendron (*Rhododendron* sp.), and poison ivy (*Toxicodendron radicans*) (Matosziuk et al. 2020; NPS 2019).

All sample preparation and analysis occurred within the Organic Matter Spectroscopy or Sedimentology Laboratories at the University of Colorado Boulder located in Boulder, CO. The photodegradation experiment occurred outdoors at the University of Colorado Boulder's Skywatch Observatory (40°00'40"N, 105°14'32"W) at an elevation of 1660m (<https://skywatch.colorado.edu/>).

Unburned organic matter (OM), consisting primarily of fallen leaf litter and loose topsoil, was collected and stored in large polyethylene plastic bags. Topsoil down to a depth of 2cm was collected from the same sites (Blank et al. 1996). Samples were gathered in August 2018 and due to heavy precipitation in the week prior to sample collection, the samples were airdried for 48 hours onsite. Upon returning to Boulder, CO the soils were freeze dried and the leaf samples were dried in an oven at 60°C for 48 hours to ensure uniform drying (Blank et al. 1996; Hansen et al. 2016).

Burning

Combining methods and lessons learned from previous studies (Blank et al. 1994; Blank et al. 1996; Myers-Pigg et al. 2017; Schneider et al. 2010; Brown et al. 2006; Blank et al. 1996; Santín et al. 2017; Wagner et al. 2018; Novotny et al. 2015; Wiedemeier et al. 2016), artificial PyC was produced by burning OM (leaves and topsoil) at various temperatures to isolate distinct portions of the PyC spectrum starting at 200°C (Schneider et al. 2010; Blank et al. 1994; Novotny et al.

2015). The following seven temperature treatments were used: unburned, outside, 200, 300, 400, 550, and 700°C. The temperature of the outside burns was logged using two thermocouple probes attached to a Gain Express 4 Channel K Type Thermometer. Max temperatures reached occurred between 300 and 475°C. All remaining samples were pyrolyzed using a muffle furnace. Leaves and soils were burned separately but using the same method. Porcelain dishes were pre-weighed and approximately 15g or 30g (depending on dish size) of leaves were placed in the dish and left uncovered. Between two to four dishes were placed into a preheated muffle furnace to minimize temperature drops. Samples were heated for 15 minutes. After 15 minutes the samples remained in the open furnace until cool enough to be transferred to a desiccator. Once cooled completely the samples were weighed and mass loss was recorded.

When attempting to simulate wildfire PyC production using a muffle furnace, previous studies have mentioned the most significant differences include that wildfire charcoals form under variable but higher max temperatures (500-950°C), are exposed to atmospheric gas (ie. oxygen availability) and endure shorter heating durations (Santín et al. 2017; Brown et al. 2006; Novotny et al. 2015; Blank et al. 1994; Blank et al. 1996). PyC production from wildfires result in PyC that is more heterogeneous; whereas, slow pyrolysis occurs under controlled and stable conditions that are oxygen deprived, endure longer heating durations, and experience lower maximum temperatures (300-700°C) (Santín et al. 2017). Wildfire chars have higher O:C and H:C ratios,

Leaching



Figure 4: Batch leaching of the separate burn treatments. From left to right: solution blank, outside burn, 700, 550, 400, 300, 200°C, and unburned. The burned OM is leaching in a solution of sodium bicarbonate and formaldehyde.

Each of the temperature treatments: unburned, outside burn, and the five temperature intervals, in addition to a solution blank were each leached separately in 20L Nalgene carboys, making a total of 8 samples solutions. Each Nalgene Jug was autoclaved and filled with a solution that included 15L of autoclaved 18.2 MΩ deionized water, 0.001 M sodium bicarbonate (NaHCO_3), and 0.04% formaldehyde (CH_2O). Throughout the entire experiment, all bottles, carboys, water, and other eligible equipment was autoclaved to maintain a sterile environment and combat microbial influence. The sodium bicarbonate was added to buffer the pH and to inoculate the water with essential cations and anions to mimic the ionic strength of natural systems (Wickland et al. 2007;

Gabor et al. 2015; Steele and Aitkenhead-Peterson 2013; Trevors 1996). The formaldehyde was added to inhibit microbial growth and interference given the longer leaching and exposure times during the photodegradation portion of the experiment (Tuominen et al. 1994; Hader et al. 2003). For each temperature treatment, 225g of leaves and 75g of soil were added to the respective carboy. Carboys were loosely covered in foil and stirred frequently to prevent anoxia. The three-day leach period occurred between July 26-29th, 2019.

While most of the DOM is leached within the first day (Steele and Aitkenhead-Peterson 2013; Gunnarsson et al. 1988; Petersen and Cummins 1974; Qualls et al. 1991), depending on the type of vegetation and conditions this leaching period can be extended to 72 hours (McDowell and Fisher 1976) or up to 5 days (Otsuki and Wetzel 1974). Given that we were intentionally leaching more recalcitrant, PyC compounds, we decided on a three-day leaching period.

The carboys were mixed daily in addition to measuring pH, temperature, and conductivity. Hanna probes HI 9025 and HI 9033 were used to measure pH and conductivity respectively. Within the first day of leaching the 400, 550, and 700°C samples pH's rose to 8.84, 9.78, and 10.32, respectively. In order to bring down the pH to more typical stream levels between 5-8, we added hydrochloric acid (HCl) periodically for the remainder of the leaching period to keep the pH within an acceptable range. The final volumes of HCl added to the 400, 550, and 700°C carboys were 50mL, 230mL, and 625mL, respectively.

After the three-day leaching period, all the samples were filtered by first straining through an aluminum mesh and then through combusted 0.7µm Whatman GFF filters using Geotech

Acrylic Filter towers and peristaltic pumps (Cleveland et al. 2004). The dissolved fraction was then divided out into 250mL Nalgene Wide-Mouth PMP Bottles. Each bottle was filled with 200mL of the respective sample solution.

Table 2 shows the sample breakdown. Each burn treatment had six replicate samples for each exposure length of 1, 4, 7, 14, and 25 days, where three replicates were for the dark control and three replicates were for light exposed samples. Day 0 was the only exception with only three replicates for the dark control samples. This came out to a total of 264 samples.

Table 2: Sample matrix of burn treatment and solar radiation exposure									
Solar radiation exposure	Burn treatment								
	solution blank	unburned	outdoor	200°C	300°C	400°C	550°C	700°C	
0 days	3	3	3	3	3	3	3	3	3
1 day	6	6	6	6	6	6	6	6	6
4 days	6	6	6	6	6	6	6	6	6
7 days	6	6	6	6	6	6	6	6	6
14 days	6	6	6	6	6	6	6	6	6
25 days	6	6	6	6	6	6	6	6	6
total samples	264								

* Each treatment-exposure combination was performed in triplicate with both light-exposed and dark-control samples, with the exception of day 0 which only included dark control triplicates

Photodegradation – incubation period

All samples were placed outside within the protected area of the University of Colorado Boulder’s Skywatch Observatory and exposed to natural sunlight for various exposure times ranging from zero to 25 days. While research has shown that more than 70% of DOM degrades within the first 10 days (Cleveland et al. 2004), PyOM is known to be more recalcitrant which is why the exposure period was extended to 25 days. Many previous studies have performed photodegradation



Figure 5: Light-exposed leachates were placed on wire racks within the Skywatch Observatory. Samples were opened and turned daily. The leachates were placed in the same order on each rack in triplicate groups. The left most rack, starting from top to bottom and left to right, the leachates appear as: solution blank, 200°C, unburned, 300°C, outside, 400, 550, and 700°C.

experiments using solar simulators (Jaffe et al. 2004; Hansen et al. 2016; Cory et al. 2007; McKay and Rosario-Ortiz 2015). This experiment took place outside in natural sunlight, so samples underwent natural diel cycles. A diel cycle is important in controlling many in-stream processes. For metals, the diel cycle incorporates alternating photoreduction and dissolution processes followed by oxidation and precipitation processes (Hrcir and McKnight 1998; McKnight and Duren 2004). This photodegradation experiment took place in Boulder, Colorado from July 30th until August 23rd, 2019. The bottles containing the light-exposed leachates were laid sideways on wire racks, as demonstrated in figure 5, and the dark samples were wrapped in aluminum foil and placed in storage bins. All bottles were shaken, flipped, and opened daily to minimize anoxic conditions. The pH, temperature, and conductivity of the samples was checked regularly – every

day for the first few days of the experiment and then every three days. Temperatures were monitored but it has been shown that temperature does not strongly impact photochemical processes when temperatures remain within the normal range of surface waters (Cory et al. 2007).

Daily UVB and PAR data was downloaded from a nearby NOAA Earth System Research Laboratory (ESRL) Table Mountain site located in Boulder, CO. The UVB instrument is a Yankee Environmental Systems model UVB-1 radiometer and the PAR sensor is a LI-COR LI-190R Quantum sensor (Augustine et al. 2000). There was no available UVA data from the ESRL site, so daily UVA data was downloaded from a Colorado State University Natural Resource Ecology Laboratory (NREL) site location in Nunn, CO (elevation 1577 m) (Gao et al. 2010, data access at <https://uvb.nrel.colostate.edu/UVB/>). The UVA data was collected using an Ultraviolet Multifilter Rotating Shadowband Radiometer (UV-MFRSR). The UVB and PAR data was collected over 24 hours. The UVA data was only collected from between 6:00am to 6:00pm. The UVA, UVB, and PAR data was combined in order to report total daily solar radiation exposure relevant to DOM photolysis. The total UV Radiation (UVR) represents the cumulative UVA and UVB, which respectively account for 50% and 25% of DOM photolysis (Hader et al. 2003). The remaining 25% of DOM photolysis can be attributed to PAR, which lies within the visible spectrum so is much larger in magnitude (Hader et al. 2003).

At the end of each solar exposure period, samples were filtered through a 0.7 μ m combusted GFF filter between 3pm-6pm on the appropriate filter day. The light-exposed samples were filtered outside. Immediately after filtering, 24mL of sample was added to a dark centrifuge tube already containing 1mL of a reagent in order to be analyzed for hydrogen peroxide concentrations while

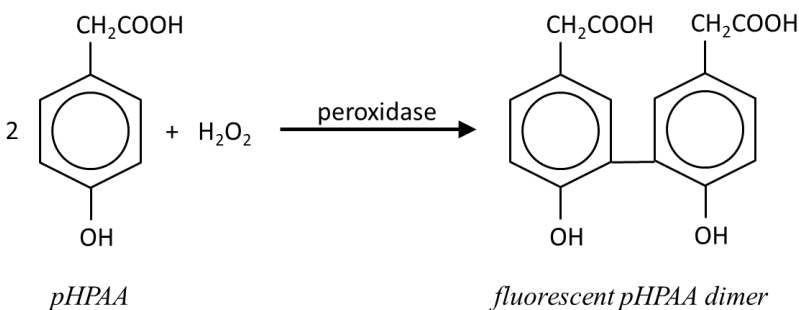
the remaining filtered samples were poured into combusted amber bottles to be analyzed. All samples were stored in a fridge at 4°C.

Analyses

An Agilent UV-visible spectrophotometer was used to collect absorbance data and a Horiba Jobin Yvon FluoroMax-3 spectrofluorometer equipped with DataMax data acquisition software were used for all fluorescence analysis. Prior to any fluorescence analysis, all samples were diluted accordingly to an absorbance below 0.2 at the 254nm wavelength.

i. Photochemical analysis

Photochemistry was confirmed by monitoring the photochemical formation of hydrogen peroxide (H_2O_2) via constant wavelength fluorescence spectroscopy. This H_2O_2 detection technique was adopted from the peroxidase enzyme fluorescent technique of Kok et al. (1986) and Lazrus et al.



(1985). This technique relies on the reaction of H_2O_2 , P-hydroxyphenylacetic acid (pHPAA), and peroxidase to form an easily detectable pHPAA fluorescent dimer (Fig.6). This reaction is

Figure 6: Figure adapted from Kok et al. Oxidation of pHPAA by H_2O_2 and peroxidase into the fluorescent pHPAA dimer (Kok et al. 1986; Schylte-Ladbeck et al. 2003)

complete within one minute (Kok et al. 1986). The concentration of this fluorophore is then detected using a spectrofluorometer.

This technique involves adding a reagent (Table 3) to sample in order to produce and fix the concentrations of a fluorophore (pHPAA dimer) (Fig. 6) that can be measured within 24 hours on a fluorometer. Our samples were deliberately leached to have high concentrations of DOM, so we anticipated high concentrations of H₂O₂. For this reason, we employed a 1:25 volume dilution of reagent to sample to ensure there was enough pHPAA (Kok et al. 1986). The reagent has a shelf life of four days, after which the activity of the peroxidase decreases. Therefore, the reagent was made fresh for each filtration day, except for day 0 and day 1 samples.

Table 3: Hydrogen Peroxide Reagent Composition

Chemical	Concentration	Purpose
Tris (hydroxymethyl) aminomethane*	0.5 M	Buffer to maintain pH of final solution between 8 and 9. Ensures the best stability of reagent and reaction products.
Na ₂ EDTA	0.005 M	Mask interferences by complexing with transitioning metals
Formaldehyde (HCHO)*	0.26 M	Reduce interference from hydroxymethanesulfonate
P-hydroxyphenylacetic acid (pHPAA)*	0.15 M	Includes active components in reagent
Horseradish peroxidase*	150 units / 100mL solution	Includes active components in reagent.
NaOH		Use as needed to adjust reagent pH to at least 9

*Fisher brand. **Sigma-Aldrich. Adapted from Kok et al. 1986.

Leachates were filtered between 3-6pm on respective days. All light-exposed samples were filtered outside, given that H₂O₂ is a transient species. During the filtration process, samples were filtered through 0.7µm pre-combusted GFF filters. Immediately after the sample passed

completely through the filter, 24 mL was pipetted into dark, screw-cap polyethylene centrifuge tubes that already contained 1mL of reagent. The sample-reagent solutions were then kept refrigerated until analyzed the next morning.

Prior to analyzing, all samples were adjusted to a pH of at least 10 using NaOH. Samples were diluted accordingly to an absorbance below 0.2 using a UV-visible spectrophotometer. A constant wavelength analysis application was used to detect the signal of the pHPAA dimer at excitation 320nm and emission 400nm. A standard curve was generated using serial dilutions of hydrogen peroxide concentrations (0.05, 0.01, 0.005, 0.001, 0.0005, 0.0001 mM H₂O₂) mixed with the reagent, and pH adjusted (>10).

ii. Excitation-Emission Matrices (EEMs)

A Horiba Jobin Yvon FluoroMax-3 spectrofluorometer and DataMax data acquisition software were used for all fluorescence analysis. The 3D EEM scans were collected over the paired excitation-emission wavelengths spanning an excitation range of 240 – 450nm at increments of 10nm and an emission range of 300 – 550nm at increments of 2nm. A blank sample of 18.2 MΩ water was subtracted from all EEM scans. Matlab was used to instrument correct all EEM scans and normalize with the Raman peak. Statistical analyses and figures were generated in Matlab and RStudio.

RESULTS AND DISCUSSION

Quantifying solar radiation

Figure 7 illustrates the daily variation of solar radiation relevant to DOM photolysis (UVA, UVB, and photosynthetically active radiation (PAR)). Table 4 showcases the cumulative solar radiation to which the leachates had been exposed to at each time point (day 0-25). Both UV-only (UVA and UVB) and total radiation (UVA, UVB, and PAR) were reported for the sake of comparing to other studies that only report UV radiation. All day 0's and all dark samples remained at 0 W/m² throughout the experiment, so the radiation values only apply to the light-exposed samples. As previously stated, the values reported have been adjusted to reflect the 50%, 25%, and 25% contributions of UVA, UVB, and PAR, respectively, to DOM photolysis (Hader et al. 2003). PAR lies within the visible spectrum, which is much larger in magnitude hence why the total radiation values far exceed the UVR numbers (Hader et al. 2003). Solar radiation is expected to vary from

day to day, but the incoming total radiation remained above 20,000 W/m² throughout the entire experiment with only four days (July 29th, August 3rd, 9th, and 13th) exceeding 45,000 W/m².

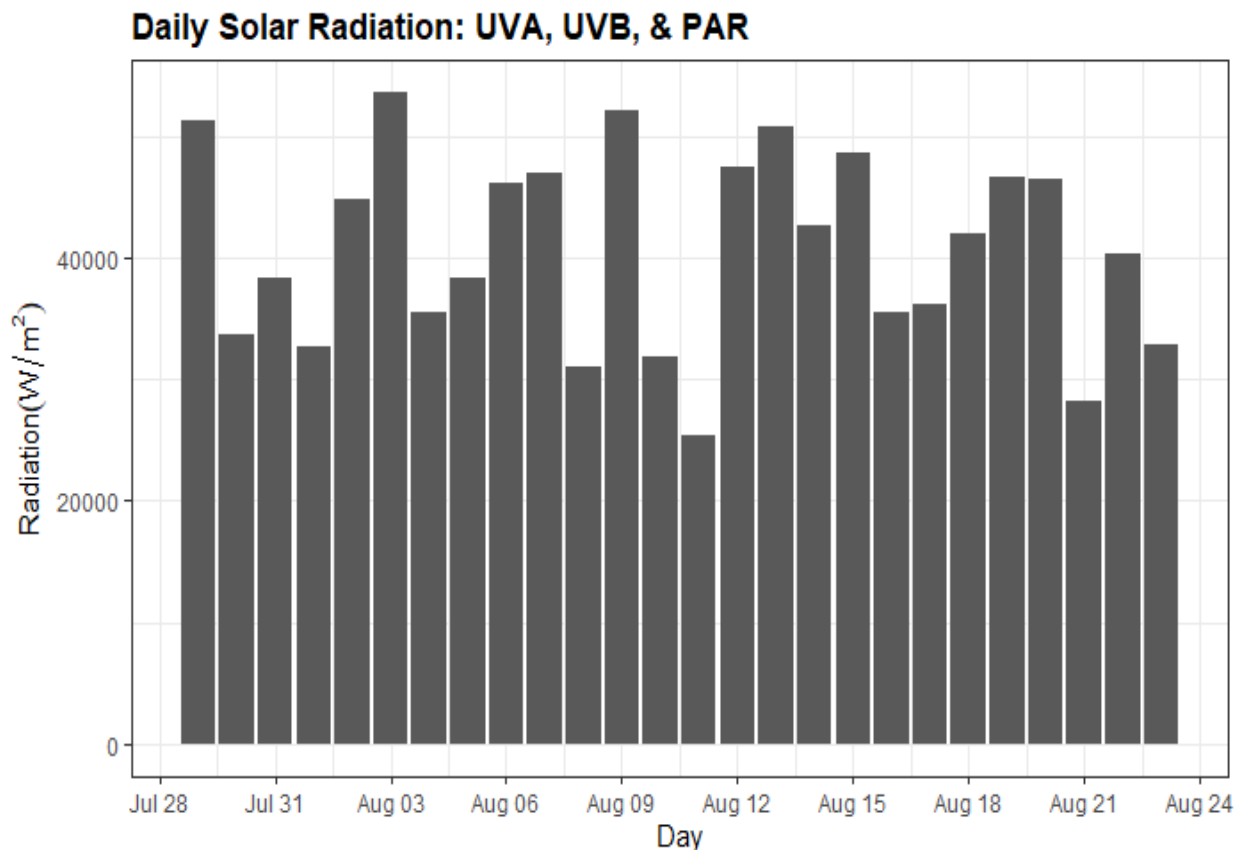


Figure 7: Daily solar radiation throughout the duration of the photoexposure experiment. Missing UVA data on July 31st.

Table 4: Cumulative Solar Radiation		
Day	UV Radiation (W/m ²) [UVA & UVB]	Total Radiation (W/m ²) [UVA, UVB, & PAR]
0	0	0
1	443	48,651
4	1,365	98,693
7	2,725	220,833
14	5,474	447,980
25	9,630	746,686

UV₂₅₄ absorption

Absorbance of natural water systems is largely dependent upon DOC concentrations, reflective of conjugated aromatic CDOM moieties that strongly absorb in the UV spectrum, peaking at 254nm (Osburn et al. 2016; Peacock et al. 2014; Lei et al. 2019). In this study, UV absorption at 254nm (UV₂₅₄) was used as a proxy for remaining DOM concentration of the leachate instead of total organic carbon (TOC). The addition of formaldehyde as an antimicrobial agent significantly elevated the TOC data whereas the formaldehyde has much less of an impact on the UV₂₅₄ absorption (Loh et al. 2007; Peacock et al. 2014). Reported UV₂₅₄ values account for dilutions required to reduce UV₂₅₄ values to below 0.2 absorbance in order to avoid any inner filter effect (Coble et al. 2014; Miller et al. 2010).

The unburned and 200°C leachates exhibited the highest UV absorbance, followed by the outside, 300, 400, 550, and 700°C leachates. All light-exposed samples exhibited reduced absorbance values compared to the dark-control counterparts (Figure 8). In addition, absorbance of all light-exposed samples within a given treatment decreased with increased exposure to solar radiation, indicating that the chromophoric DOM was degrading over time throughout the experiment.

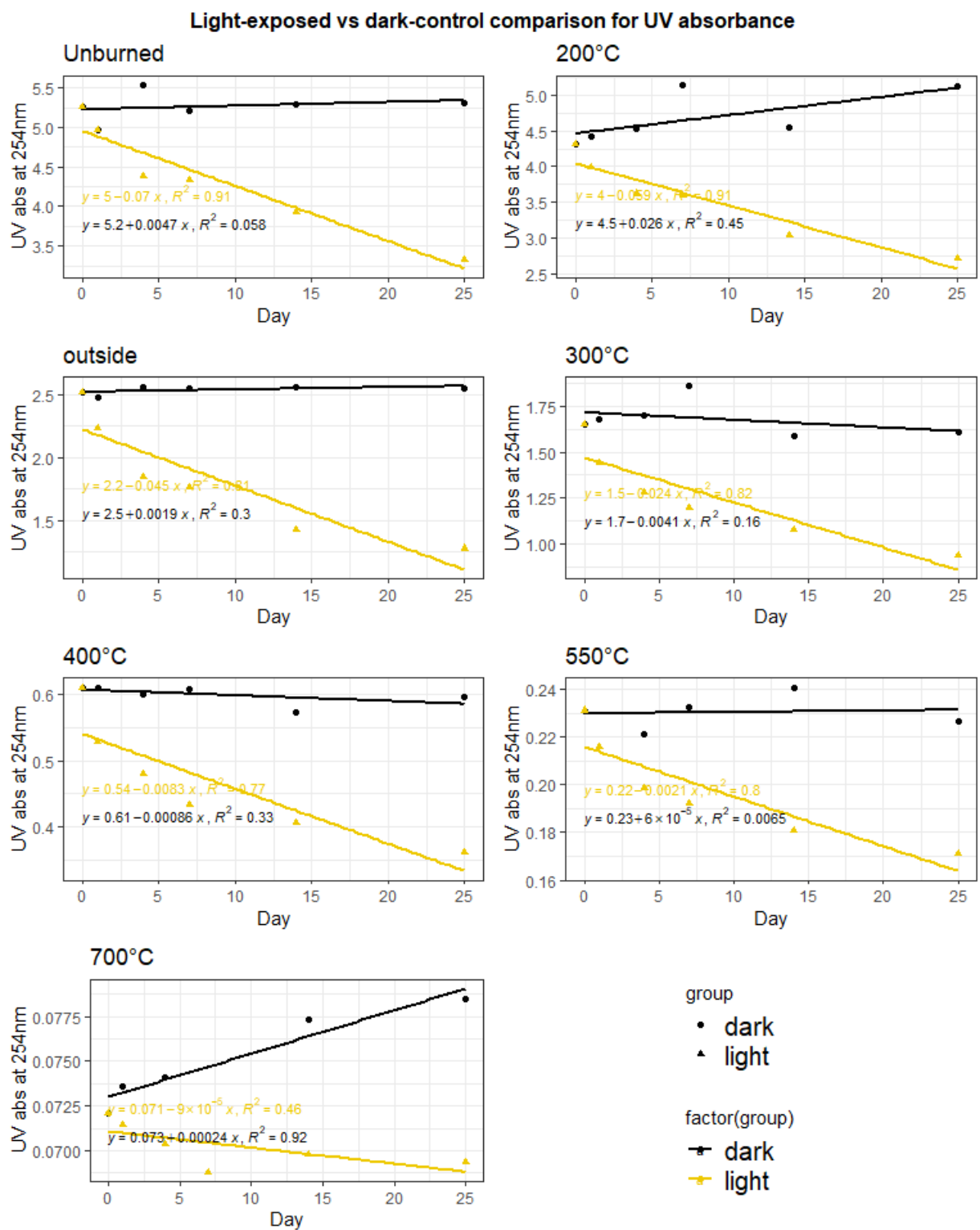


Figure 8: UV absorbance throughout 25-day experiment

Hydrogen peroxide: a confirmation of photolysis

Hydrogen peroxide (H_2O_2) is a byproduct of DOM photolysis and therefore an indicator of photochemistry. H_2O_2 does not accumulate, instead H_2O_2 is a reactive species that forms in the presence of UV light and oxygen and is then available to react with other dissolved organic molecules. Figure 9 compares the hydrogen peroxide concentrations of all the light-exposed versus dark-control samples across various treatments with a fixed hydrogen peroxide axis.

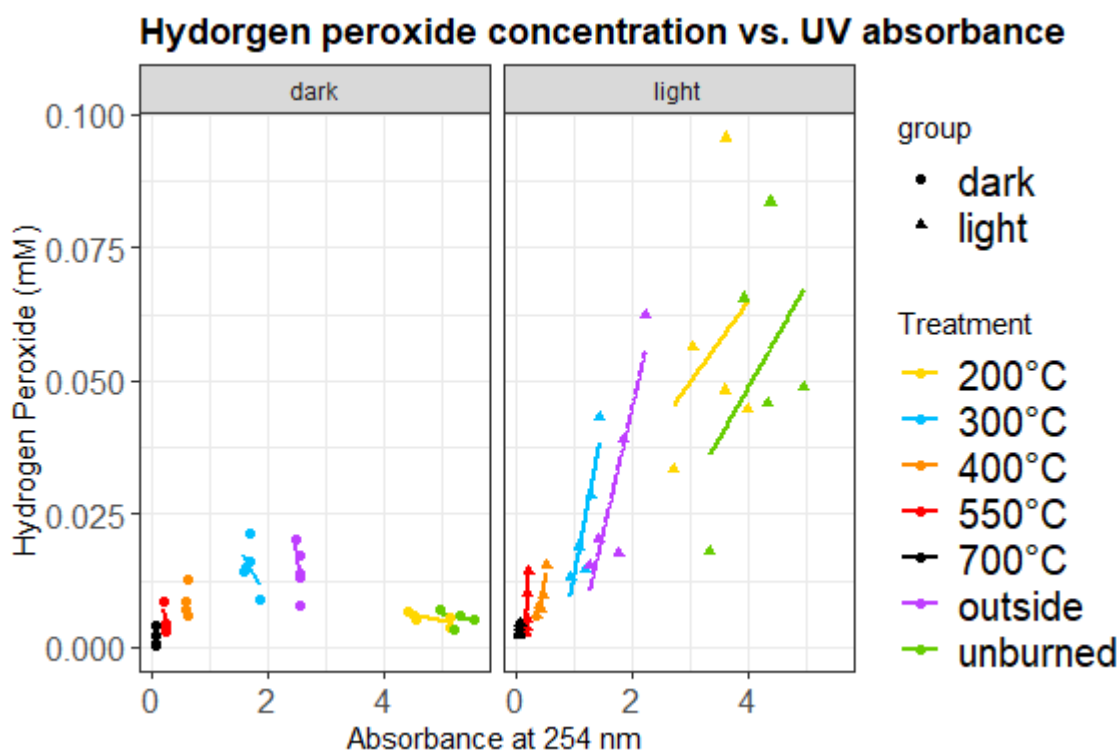


Figure 9: Hydrogen Peroxide concentrations compare to UV absorbance throughout the duration of the experiment.

The plots in figure 9 illustrate that overall much more H_2O_2 production is occurring in the light-exposed samples compared to the dark control samples for the unburned, outside, 200, and 300°C leachates. For the 400 and 550°C leachates, the H_2O_2 production is comparable in the light

and dark, and the 700°C leachate has the lowest H₂O₂ production. Meaning the DPyC is degrading due to UV light exposure. This also shows that the DOM leachate from lower temperature treatments is more susceptible to photolysis – meaning that as OM undergoes increasing thermal alteration, it becomes less susceptible to photodegradation. While this trend is to be expected, our results highlight that even the higher temperature treatments are still susceptible to photodegradation – which challenges previous conceptions that these compounds remain recalcitrant and inert.

Figure 10 illustrates the temporal decrease in H₂O₂ concentrations for each temperature treatment, again showing that all light-exposed leachates generally produced higher H₂O₂ concentrations than their dark counterparts. There are only 4 exceptions to this, which all occurred on the final day 25 for the 300, 400, 550°C, and outside treatments. These exceptions are likely a result of depletion of the overall reactant DOM pool, meaning if there is less DOM leachate to react then less H₂O₂ will form. Throughout most of the experiment, there is an exponential decay relationship between solar radiation exposure time and H₂O₂ concentration and absorbance: when solar radiation exposure time increases both H₂O₂ concentration and absorbance decrease. This relationship weakens with both the unburned and 200°C samples which exhibit maximum H₂O₂ concentrations on day four indicating a short-term spike in photochemistry.

Both Figures 9 and 10 reveal that the unburned and outside burn seem to pair with the 200°C and the 300°C, respectively. The 300°C and outside pairing validates that our burn methods and results are applicable to OM produced by wildfires. Additional qualitative analysis would provide additional insight into differentiating between muffle furnace and outside production.

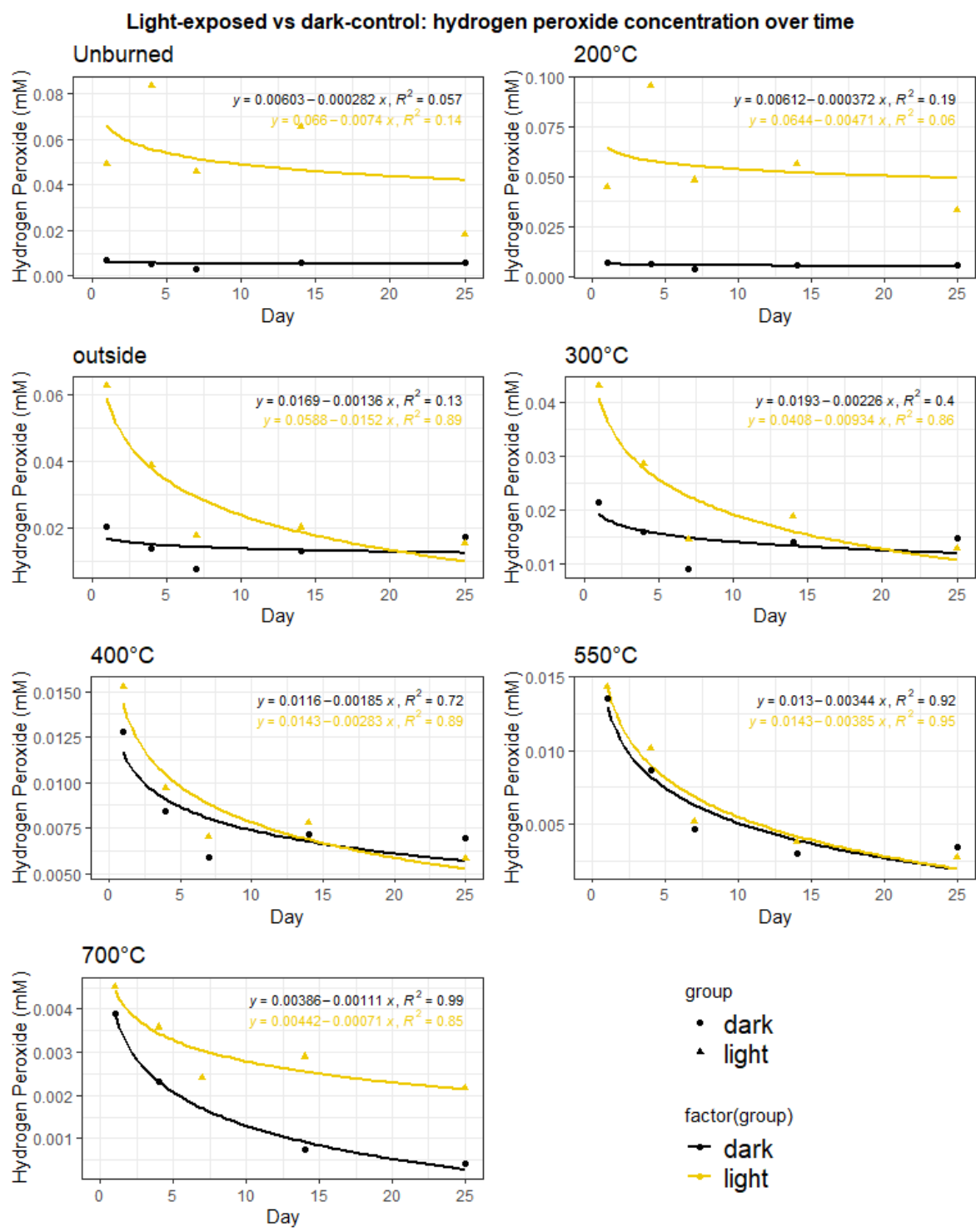


Figure 10: Hydrogen peroxide concentrations over time

Figure 11 illustrates the ratio of hydrogen peroxide concentrations to UV absorbance ($H_2O_2:UV_{254}$) throughout the duration of the experiment. All leachates, including both dark-controls and light-exposed, exhibit a declining $H_2O_2:UV_{254}$. The 550 and 700°C leachates experience the steepest decline, while maintaining the highest values throughout most of the experiment. The 200°C and unburned leachates are much darker in color and have much higher UV_{254} values, which would result in lower ratio values. These trends could also reflect potential attenuation – where the higher temperature leachates were clearer and the lower temperature leachates were darker in color, which could have impacted the depth of penetration of solar radiation. Overall, the light-exposed leachates maintain higher values than their dark-control

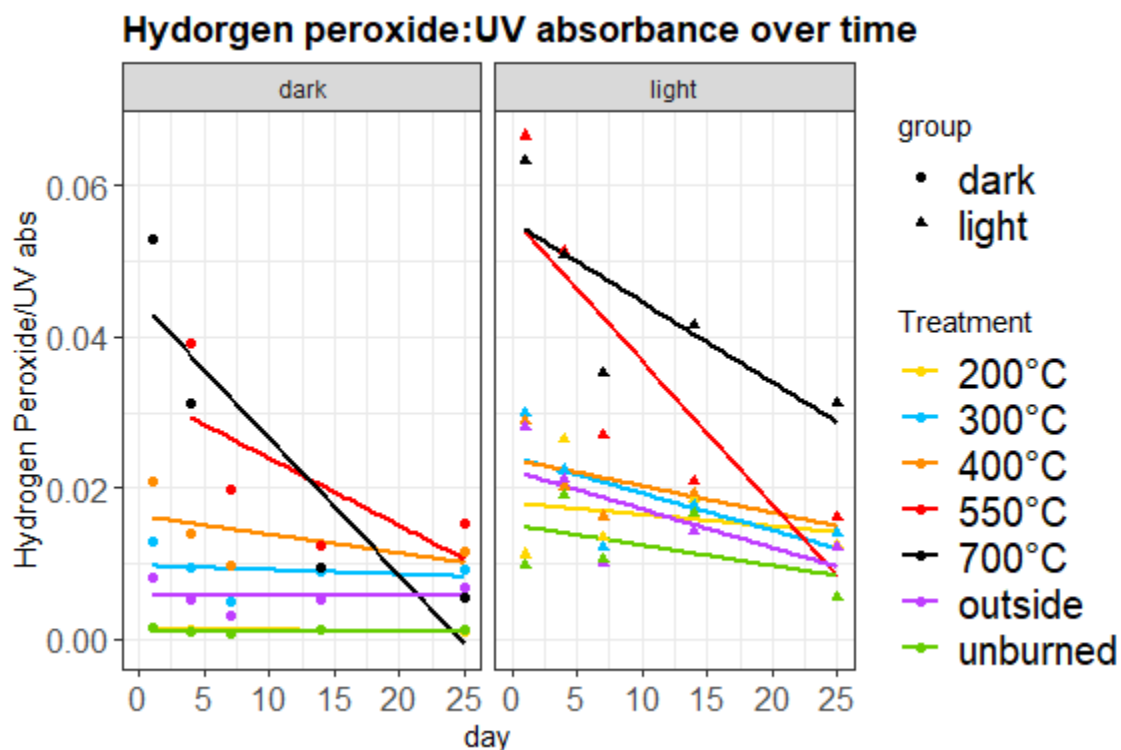


Figure 11: Ratio of hydrogen peroxide concentration to UV absorbance over time

counterparts but both groups exhibit similar trends. This could indicate that there are other oxidants produced as a result of the PyC formation process that are independent of light-exposure.

Fluorescence Spectroscopy

i. Excitation-emission matrices

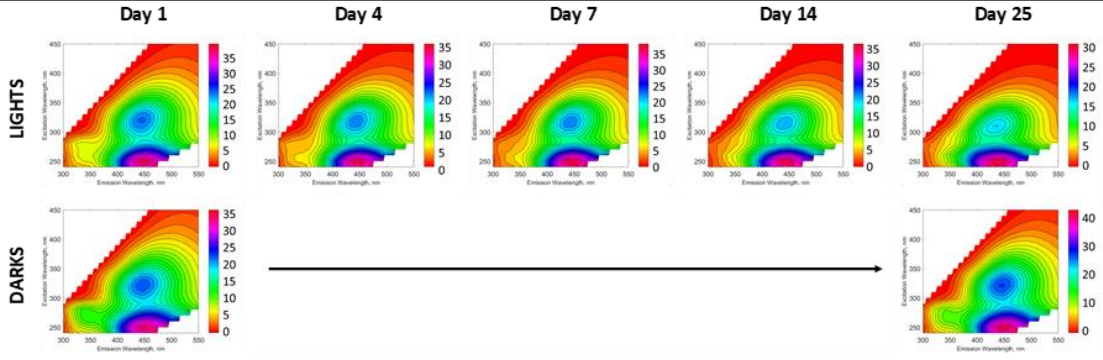
Figure 12 illustrates the temporal shifts in the excitation-emission matrices (EEMs) of all burn treatments: unburned, outside, 200, 300, 400, 550, and 700°C. Fluorescence intensity is measured in Raman units. Within each temperature group, the light-exposed samples are in the top row, the dark-control samples are in the bottom row, and the UV-exposure time increases from light to right. Dark sample EEMs for days 4, 7, and 14 were omitted because no significant changes occurred. An important distinction to notice is that the intensity scale changes over time and between the light versus dark samples. The total fluorescence intensity of the EEM decreases significantly for all light-exposed leachates, indicating a decrease in both CDOM and FDOM.

The unburned-200°C and outside-300°C pairings emerged again throughout the fluorescence spectroscopy results and can visually be observed in the EEMs (figure 12). There is a distinct reduction in fluorescence intensity in the humic peak regions for the light-exposed samples, consistent with the decrease in absorbance. The overall reduction in fluorescence intensity along with greater bleaching of the humic peak regions is expected when DOM has been photodegraded (Coble et al. 2014; Moran et al. 2000; Coble 1996). Studies have shown that as

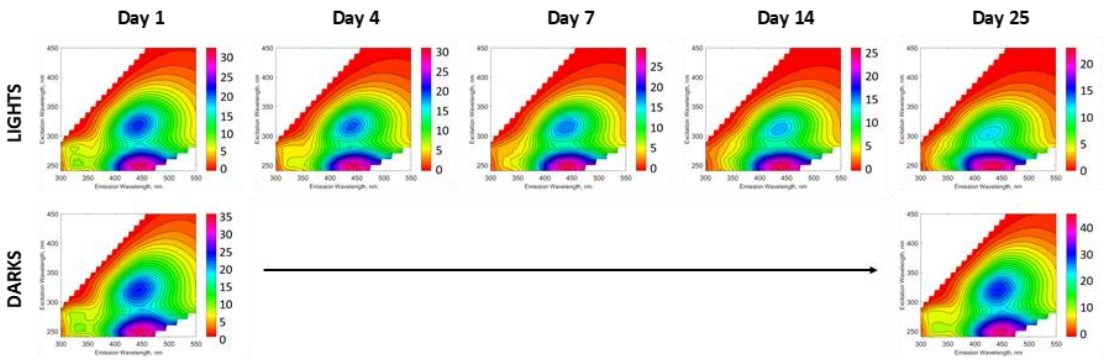
DOM is photodegraded, the longwave emission should be reduced as a result of polyaromatic compounds breaking apart, which decreases the π -electron system (Coble et al. 2014; Senesi and D’Orazio 2005). This preferential decrease at the longer emission wavelengths is also referred to as blue-shifting (Coble et al. 2014). Previous studies have suggested that this paired decrease in humic peak and increase in lower wavelengths has been associated with the formation of new chromophores (Coble et al. 2014; Biers et al. 2007). Additionally, the continued destruction of polyaromatic compounds eventually leads to the reduction of generated reactive oxygen species (ROS), demonstrated by the reduction of the H_2O_2 , that also correlate with blue-shifting (Coble et al. 2014; O’Sullivan et al. 2005).

This shift in emission wavelengths within the humic peak region often reveals information about DOM aromaticity (degree of humification, HIX), hydrophobicity, precursor material (fluorescence index, FI), source material (freshness index, $\beta:\alpha$), and electron shuttling ability (Redox Index, RI) (Coble et al. 2014). These fluorescence signals are further explored using PARAFAC components that examine regions within the EEMs.

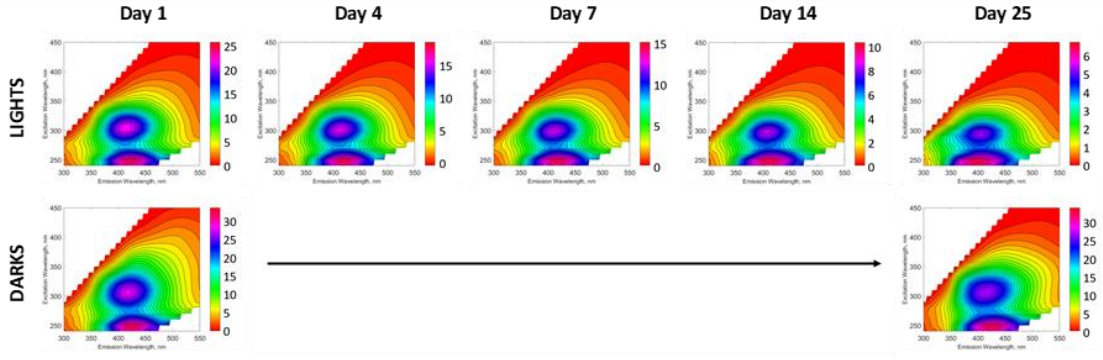
Unburned



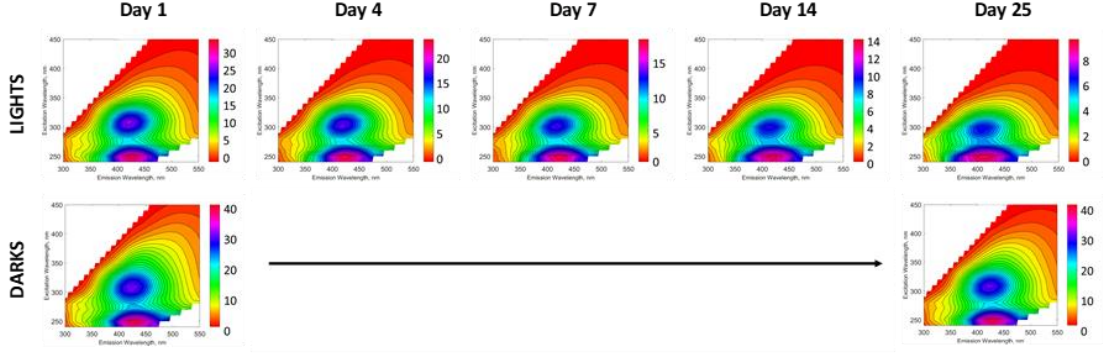
200°C



300°C



Outside



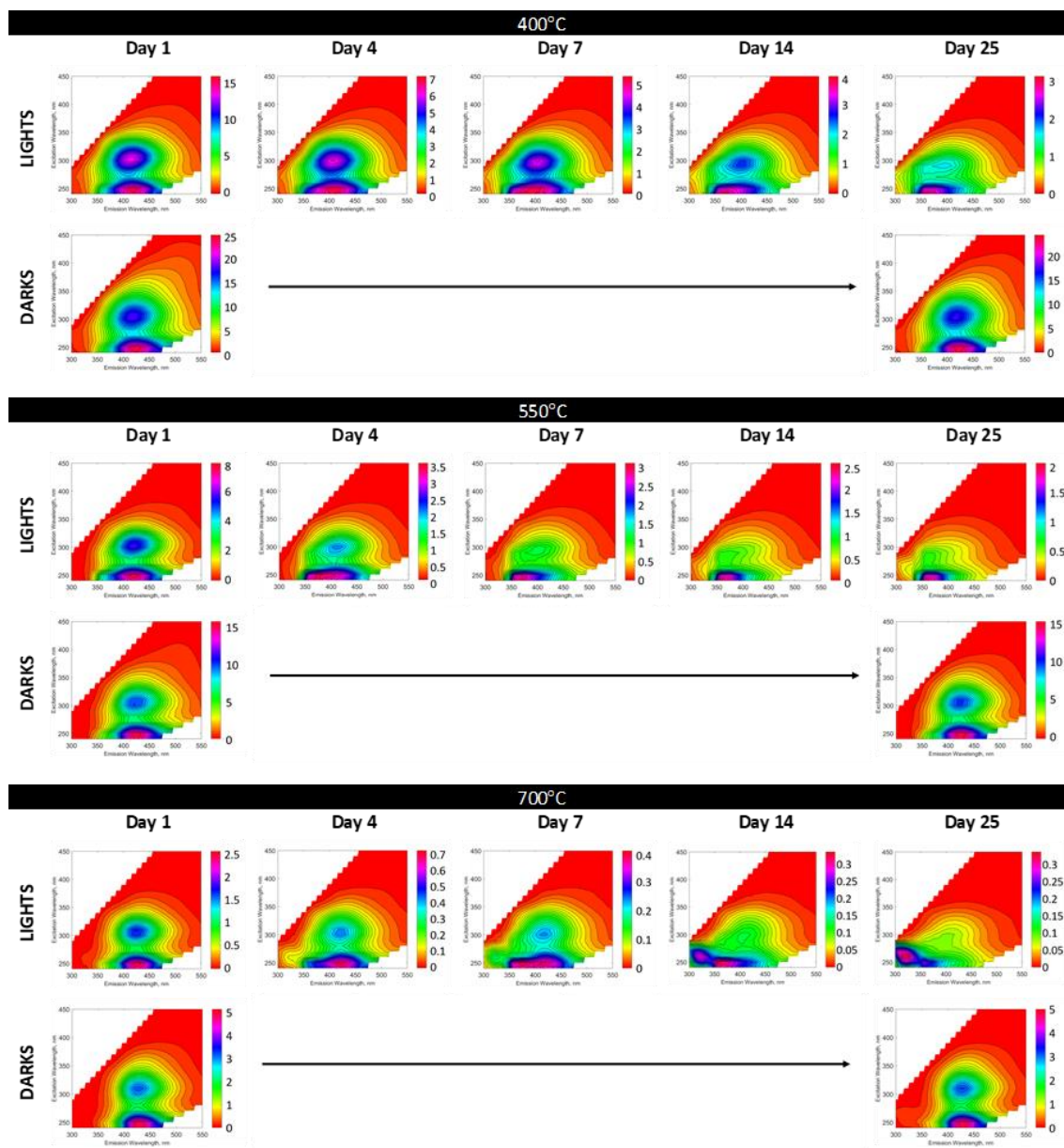


Figure 12: Excitation-emission matrix comparison across burn treatments and light-exposed versus dark-control groups.

ii. pH effects

The influence of pH on the fluorescence of certain DOM moieties varies. In some instances, more acidic conditions ($\text{pH} < 5$) have been shown to decrease fluorescence intensity and cause blue shifting (Coble et al. 2014; Laane 1982). Overall, the dark-control group remained at a slightly higher pH than their light-exposed counterpart samples, likely due to the production of organic acids as a result of photodegradation (Figure 13). The intensity of the dark-control leachates remains relatively constant throughout all treatment groups for the entire 25-days. The light-exposed 200°C and unburned samples exhibited a significant decrease in pH over the 25-day exposure period, both starting around a pH of 6 and ending below a pH of 4.5, whereas the pH of the remaining treatment leachates remained relatively steady and slightly basic (between 7 and

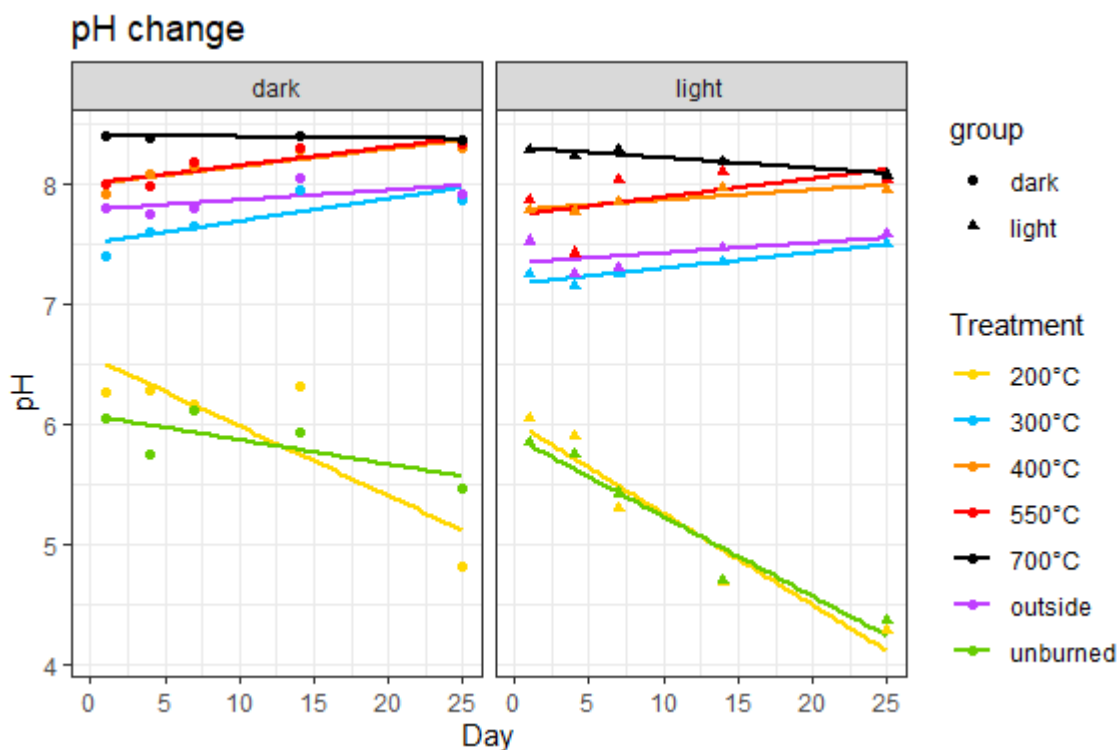


Figure 13: pH of the various treatments and groups throughout the 25-day experiment.

8.5). The more neutral leachates (outside, 300, 400, 550, and 700°C) did experience greater shifts and diminished fluorescence intensity; however, these changes only occurred in the light-exposed groups and not in the dark-exposed groups, indicating that the pH had minimal effects.

iii. Fluorescence indices

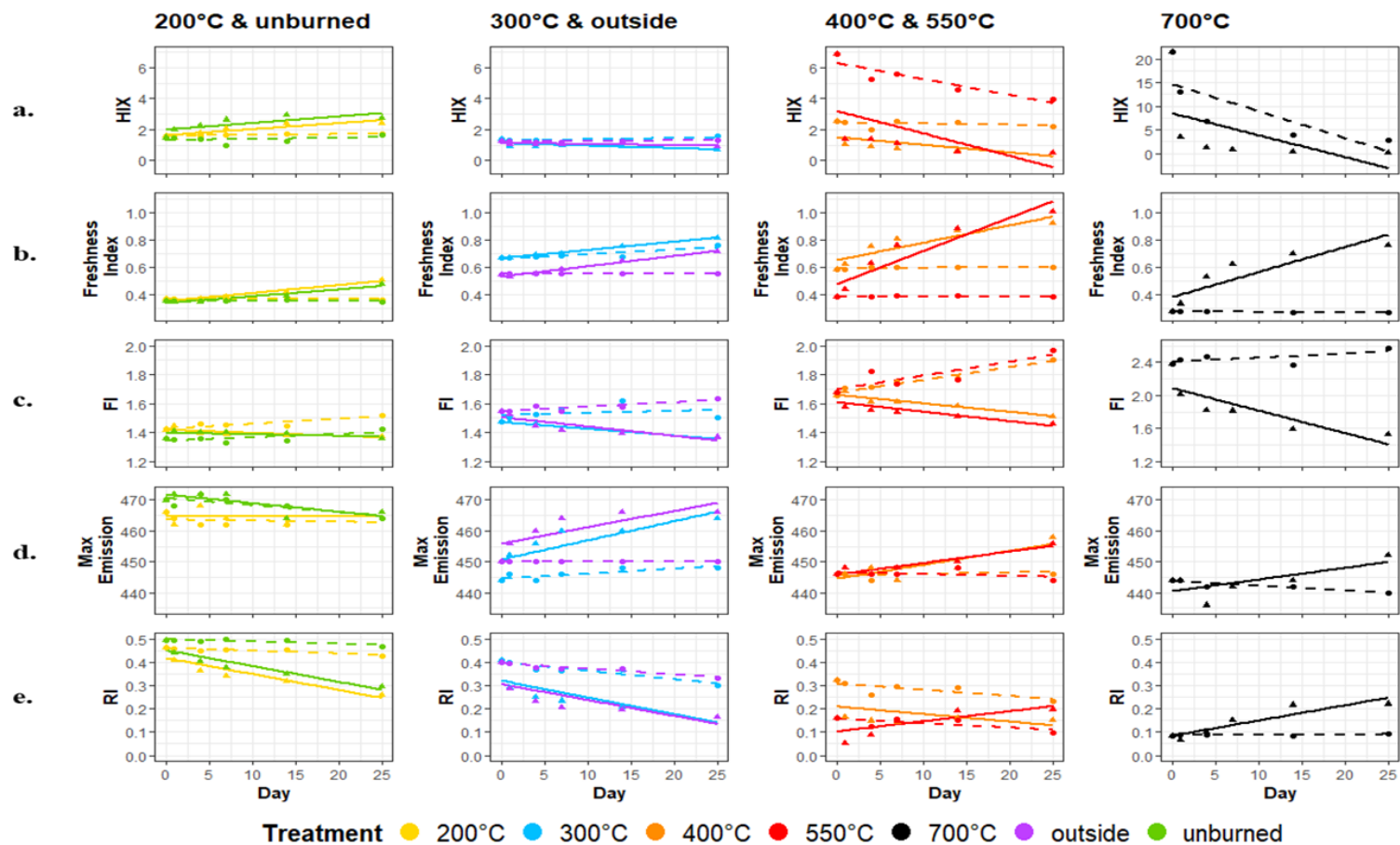


Figure 14: Fluorescence indices over time. All axes scales are the same except for the HIX and FI maximums for the 700 °C treatment. Each column represents various burn treatments and each row represents a fluorescence index. The humification index (HIX) is the first row (14-a), freshness index is the second row (14-b), fluorescence index (FI) is the third row (14-c), Maximum emission at 370nm is the fourth row (14-d), and redox index (RI) is the fifth row (14-e).

Table 5 Summary of fluorescence indices and PARAFAC components for Day 14

Group Treatment	Light							Dark						
	unburned	200°C	300°C	outside	400°C	550°C	700°C	unburned	200°C	300°C	outside	400°C	550°C	700°C
Fluorescence Indices														
HIX	2.92	2.42	0.91	1.09	0.66	0.57	0.28	1.27	1.70	1.32	1.25	2.46	4.56	3.96
β:α	0.39	0.42	0.76	0.64	0.87	0.88	0.70	0.36	0.38	0.67	0.55	0.60	0.39	0.27
FI	1.40	1.38	1.39	1.40	1.58	1.51	1.59	1.35	1.44	1.62	1.57	1.77	1.76	2.37
max EM	464	462	460	466	448	450	444	468	462	448	450	448	448	442
RI	0.35	0.32	0.21	0.20	0.16	0.19	0.22	0.49	0.45	0.37	0.37	0.29	0.15	0.09
PARAFAC Components														
%C1	12.8%	11.7%	2.7%	4.2%	1.9%	2.2%	4.5%	14.4%	15.9%	7.4%	8.7%	6.1%	6.8%	10.1%
%C2 (Q2)	19.1%	18.0%	11.0%	13.2%	6.6%	2.6%	5.5%	16.2%	16.8%	15.4%	16.4%	17.6%	20.7%	27.0%
%C3	1.9%	2.2%	10.0%	6.9%	10.9%	5.9%	5.3%	1.8%	2.5%	11.2%	7.6%	9.0%	3.2%	0.5%
%C4 (HQ)	17.2%	15.7%	6.0%	7.2%	4.1%	9.2%	10.0%	20.5%	17.5%	9.2%	11.7%	7.0%	3.7%	0.0%
%C5 (SQ1)	2.6%	2.1%	1.4%	1.2%	0.3%	0.0%	0.0%	4.8%	4.2%	2.4%	2.6%	1.5%	0.9%	0.0%
%C6	13.1%	13.6%	9.0%	10.0%	7.0%	5.5%	7.9%	9.1%	9.2%	2.9%	4.0%	5.1%	7.6%	6.5%
%C7 (SQ2)	0.9%	0.5%	0.6%	0.6%	0.9%	1.5%	0.8%	3.6%	4.4%	3.9%	3.7%	2.4%	0.0%	0.1%
%C8 (Tryptophan)	3.4%	4.8%	8.3%	7.9%	14.6%	20.9%	18.5%	7.6%	5.3%	5.8%	5.4%	5.4%	2.7%	0.0%
%C9 (SQ3)	0.0%	0.0%	2.4%	1.4%	2.3%	0.4%	1.4%	0.1%	0.1%	5.1%	3.6%	5.7%	4.1%	4.7%
%C10	7.9%	8.3%	12.0%	12.1%	10.1%	4.9%	7.5%	5.8%	7.4%	14.5%	14.6%	16.3%	22.5%	26.9%
%C11 (Q1)	12.0%	11.9%	7.5%	9.9%	5.2%	4.2%	6.7%	8.9%	9.1%	6.7%	8.1%	7.8%	10.7%	13.1%
%C12 (Q3)	7.5%	9.6%	21.2%	20.0%	27.6%	40.1%	31.9%	4.7%	5.7%	13.1%	12.0%	14.7%	17.1%	11.0%
%C13 (Tyrosine)	1.7%	1.6%	8.0%	5.3%	8.5%	2.7%	0.0%	2.6%	1.9%	2.5%	1.5%	1.4%	0.0%	0.0%
Protein	0.051	0.064	0.163	0.133	0.231	0.236	0.185	0.102	0.072	0.082	0.070	0.067	0.027	0.000

Table 6: Percent change of fluorescence indices						
Treatment	Group	HIX	$\beta:\alpha$	FI	Max Emission	RI
200°C	light	51.4%	38.5%	-3.3%	0.0%	-43.6%
	dark	5.7%	-2.0%	7.1%	-0.4%	-7.6%
300°C	light	-48.5%	22.0%	-7.3%	4.5%	-59.2%
	dark	13.2%	13.9%	2.1%	0.9%	-25.9%
400°C	light	-80.0%	58.4%	-8.4%	2.7%	-52.9%
	dark	-13.8%	2.2%	15.2%	0.0%	-27.7%
550°C	light	-93.3%	163.5%	-13.0%	2.2%	23.8%
	dark	-42.7%	0.2%	17.5%	-0.4%	-39.4%
700°C	light	-99.3%	179.7%	-35.8%	1.8%	162.8%
	dark	-86.7%	-2.0%	8.3%	-0.9%	9.2%
outside	light	-26.5%	31.8%	-11.5%	3.6%	-58.5%
	dark	8.1%	2.4%	5.6%	0.0%	-16.9%
unburned	light	85.1%	33.9%	-0.2%	-0.9%	-40.0%
	dark	12.6%	-1.8%	4.7%	-1.3%	-5.6%

* percent change is calculated using day 0 and day 25 values

a. Humification Index (HIX)

Generally, the HIX values are fairly stable for most treatments and on the lower end of the NOM range from 0-30. The exception of the 700°C leachates which ranged from 0.14 to 21.42 (Figure 14-a). HIX is used to measure the degree of humification or maturation, so these overall lower numbers are not surprising since the leachates were generated primarily from freshly fallen leaves, meaning the parent OM had not undergone significant biogeochemical processing (ie. lacking maturation). HIX has also been associated with aromaticity and enhanced ring structure, so it would be expected that the higher temperature leachates would exhibit higher HIX values, which is the general trend we observed in our leachates.

Figure 14-a shows that in both light-and dark-groups, the higher temperature treatments experienced a more significant decrease in HIX values, indicating a decrease in aromaticity and a potential increase in oxygen-functional groups. This trend is expected as previous studies have shown that DOM photolysis leads to a decrease in the chromophoric (primarily light absorbing aromatic compounds) and fluorescent DOM fractions (Ward and Cory 2016). The 700°C HIX values drastically decrease throughout the experiment in both groups, but the decrease is more prominent in the light-exposed samples indicating that exposure to solar radiation aided in the decrease in aromaticity. Within the dark sample group, higher temperature leachates tend to have higher HIX values indicating a greater ring structure (aromaticity) and lower H:C ratios. For the light-exposed group, the temperature treatments appear opposite in order compared to the dark samples, where the lower temperature treatments exhibit higher HIX values by the end of the 25-day exposure period. Higher HIX values have also been linked to more acidic watersheds (Coble et al. 2014; Ohno et al. 2007), which might explain why the 200°C and unburned samples had higher HIX values as they became more acidic.

b. Freshness Index ($\beta:\alpha$)

All freshness index ($\beta:\alpha$) values appeared within a normal range for natural DOM (Figure 14-b). All light-exposed samples experienced an increase in $\beta:\alpha$ with increased solar radiation exposure, while the dark control samples remained relatively unchanged. The higher temperature leachates experienced the largest increase in $\beta:\alpha$, with the 700°C leachates experiencing a 180% change over the 25-day exposure period (Table 6). An increase in $\beta:\alpha$ could be indicative of microbial influence or result from the removal of humic material. Given that microbial influence was

inhibited by using sterilization measures (formaldehyde, filtering, and autoclaving), the increase in $\beta:\alpha$ is likely a result of the diminished humic peak given the decrease in fluorescence and blue-shifting observed in all the light-exposed leachates. Other DOM leachate studies have also reported an increase in $\beta:\alpha$ with photoexposure (Hansen et al. 2016).

c. Fluorescence index (FI)

Figure 14-c shows that the light-exposed samples exhibit a decrease in FI values associated with increased exposure to solar radiation and photolysis, whereas the dark-control FI values increase slightly. The higher temperature leachates were more susceptible to this decrease in FI, with the 300, 400, 550, 700°C, and outside treatment groups exhibiting the following percent changes: -7.3, -8.4, -13.0, -35.8, and -11.5%, respectively. Meanwhile the unburned and 200°C treatment groups exhibited minimal change of -0.2 and -3.3%, respectively, over the same 25-day exposure period. This is slightly inline with a previous study examining the photodegradation of Arctic DOM which found that FI was insensitive to photodegradation (Cory et al. 2007).

Most of the FI values are within a normal range for natural DOM, except for the 700°C leachates that experienced unusually high values (>2), which can be explained by shifted emission signals (Figure 14- c and d). Overall, the FI values are on the higher end of the spectrum which could indicate that recently abscised leaf litter has not undergone significant processing like that of the typical terrestrial DOM signature (Wymore et al. 2015). This is also consistent with the low HIX values. Higher FI values are typically associated with microbial precursor material but these values have also been observed in other leaf leachate studies (Wymore et al. 2015; Hansen et al.

2016), indicating that perhaps higher FI values here are representative of freshly produced material. The decreasing FI values associated with increased exposure to solar radiation, indicate a shift towards FI values that resemble more terrestrial soil-derived DOM (Hansen et al. 2016). This decrease in FI has been observed with other DOM photobleaching studies (Jaffe et al. 2004; Hansen et al. 2016). For instance, Jaffe et al (2004) reported that ‘fresh’ mangrove derived DOM exhibited higher than expected fluorescence index values (1.68) for a source that would be expected to exhibit more terrestrial end-member values, yet these values decreased throughout the photobleaching experiments indicating that photobleaching can result in decreasing FI values (ie. trend towards resembling more terrestrial-like endmembers) (Jaffe et al. 2004). We observed this same decreasing FI trend throughout this photodegradation experiment.

Table 7: Max emission signal at EX₃₇₀ comparison on day 0 and 25

		Day	
		0	25
Treatment	200°C	466.00	464.00 466.00
	300°C	444.00	448.00 464.00
	400°C	446.00	446.00 458.00
	550°C	446.00	444.00 456.00
	700°C	444.00	440.00 452.00
	Outside	450.00	450.00 466.00
	Unburned	470.00	464.00 466.00
*dark sample values are shaded.			

Previous studies have also shown that inflated FI values can correspond to the maximum humic peak emission shifting to lower emission wavelengths (Coble et al. 2014) – this trend can be observed in figure 14-d. Typically, the maximum emission should occur between 460-480nm at an excitation of 370nm (Cory et al. 2007). Table 7 shows that all unburned samples exhibited an emission peak around 470nm at excitation 370nm, which serve as a confirmation of the analysis performed. However, the emission peak at excitation 370nm shifts towards lower wavelengths as thermal alteration

increased. This shift to lower emission wavelengths (also known as blue shifted) indicates that reduced quinone-like components are weighted less in higher temperature treatments. The burned temperature treatments within the light-exposed group exhibit an increasing max emission signal throughout the experiment, potentially indicating that the photodegradation of DPyC increases the likelihood that the burned treatments will return to resembling more natural OM (NOM). This shift back towards higher emission wavelengths (red-shifting) has also been shown to occur with partial oxidation of DOM which could be indicative of increased carboxyl and hydroxyl groups (Coble et al. 2014; Senesi and D’Orazio 2005). Therefore, the decreasing FI values for the light-exposed leachates are reflective of DOM photobleaching and represent a shifting emission spectra.

More acidic conditions have also been known to increase FI values and shift the maximum emission peak at EX₃₇₀ to lower wavelengths (Coble et al. 2014). The 200°C and unburned samples exhibited a significant decrease in pH over the 25-day exposure period, both starting around a pH of 6 and ending below a pH of 4.5, whereas the pH of the remaining treatment groups remained steady and slightly basic (between 7 and 8.5) (Figure 13). When looking at the light-exposed leachates, the slightly acidic conditions could explain why the unburned leachates experienced a decrease and the 200°C leachates remained steady regarding maximum emission at EX₃₇₀ rather than experiencing an increase in maximum emission at EX₃₇₀ observed in the remaining treatment leachates. Also, the slightly acidic conditions could contribute to the unburned and 200°C leachates exhibiting very little change in FI whereas the remaining treatments exhibited decreases in FI.

d. Redox Index

Most of the RI values are within the lower range for natural DOM (<0.4), indicating that the quinone-like components are more oxidized. When considering the impact of photoexposure, there is an overall shift to lower RI values with increased exposure to solar radiation for most of the samples, indicating DPyOM is becoming increasingly degraded and oxidized. The 550 and 700°C samples are exceptions, where the RI values increase with increased exposure to solar radiation, potentially signifying that new and reduced compounds are also being generated. Photoexposure can cause polyaromatic compounds to break apart and generate reactive oxygen species (ROS), causing subsequent reactions that can continue to oxidize or reduce DOM (Coble et al. 2014). This effect can be observed in the EEMs, where the humic peak is slightly skewed in the 550 and 700°C leachates (Figure 12). This similar reducing result has been observed in a study that examined the reducing effects of microbes, which reported that within a degrading environment electron transfers can result in a shift of the main humic fluorophores to higher emission wavelengths (Coble et al. 2014; Klapper et al. 2002). Photooxidation can cause aromatic rings to open, which disrupts charge transfer reactions, resulting in longer wavelength absorption and fluorescence (Del Vecchio and Blough 2004; Coble et al. 2014).

Samples with less thermal alteration (unburned, 200°C, 300°C, and outside) exhibit a more drastic decrease (steeper, negative slope) in RI over time. This slope flattens out with the 400°C samples (which remain relatively unchanged), and then the slope switches to a steep positive slope with the 550 and 700°C samples indicating these compounds become more susceptible to

accepting electrons. The breakdown of the specific quinone-like components is discussed in the following sections.

iv. PARAFAC: Component Loading

Absolute loading is reflective of fluorescence intensity while percent loading provides the relative contribution of that component to total fluorescence (Hansen et al. 2016). When comparing the light-exposed samples to the respective dark controls, the dark control group generally exhibited no significant change in component loading, therefore the dark group was omitted in the following plots. Within the light-exposed group, most treatment leachates experience a decline in absolute loading, with a few exceptions including the unburned and 200°C leachates experiencing increases in Q3 and tryptophan. For most components, the 200°C and unburned treatments typically exhibited linear trends, whereas the remaining higher-temperature treatments followed logarithmic trends, for this reason all plots were adjusted accordingly. This shows that higher-temperature DPyC is initially more susceptible to photochemical changes, experiencing an exponential decline in quinone-like components. This could also be a result of attenuation since the 200°C and unburned samples leached the darkest solutions, which would alter the optical depth for UV light penetration.

Table 8: Percent change of absolute loadings (Day 0 to 25)

		Q1 (C11)		Q2 (C2)		Q3 (C12)	
		Light	Dark	Light	Dark	Light	Dark
Quinone-like (oxidized)	200°C	-21.6%	30.9%	-45.0%	30.0%	34.6%	23.1%
	300°C	-81.3%	12.0%	-89.7%	0.2%	-67.4%	0.7%
	400°C	-94.0%	-2.5%	-97.1%	-5.4%	-80.3%	1.9%

550°C	-97.2%	-5.0%	-99.7%	-6.2%	-79.1%	-1.3%
700°C	-97.6%	-5.3%	-99.4%	-7.0%	-85.4%	-0.3%
outside	-75.0%	9.3%	-84.0%	5.8%	-58.6%	8.0%
unburned	-5.7%	15.6%	-28.3%	15.6%	66.1%	6.0%
Average	-67.5%	7.9%	-77.6%	4.7%	-38.6%	5.4%

	SQ1 (C5)		SQ2 (C7)		SQ3 (C9)		
	Light	Dark	Light	Dark	Light	Dark	
200°C	-77.8%	1.0%	-95.8%	29.8%	--	0.0%	
300°C	-93.2%	-13.7%	-97.7%	-52.5%	-94.6%	-27.4%	
400°C	-99.8%	-44.3%	-95.2%	-31.4%	-98.3%	-7.2%	
550°C	-100.0%	-68.8%	--	0.0%	-100.0%	6.9%	
700°C	0.0%	0.0%	--	0.0%	-99.6%	4.4%	
Semiquinone-like (reduced)	outside	-92.9%	-16.1%	-97.0%	-14.4%	-95.2%	-14.5%
	unburned	-71.9%	-5.1%	-90.3%	14.0%	0.0%	0.0%
Average		-76.5%	-21.0%	-95.2%	-7.8%	-81.3%	-5.4%

	HQ (C4)		
	Light	Dark	
200°C	-60.7%	10.1%	
300°C	-92.9%	-38.7%	
400°C	-94.9%	-57.2%	
550°C	-81.6%	-85.8%	
700°C	--	0.0%	
Hydroquinone-like (reduced)	outside	-89.6%	-24.1%
	unburned	-51.8%	1.7%
Average		-78.6%	-27.7%

	Tryptophan (C8)		Tyrosine (C13)		
	Light	Dark	Light	Dark	
200°C	107.8%	7.3%	-100.0%	20.9%	
300°C	-67.5%	8.2%	-21.7%	-20.5%	
400°C	-68.9%	-4.9%	-19.3%	24.8%	
550°C	-18.3%	6.1%	--	0.0%	
700°C	--	0.0%	0.0%	0.0%	
Amino acid-like (proteins)	outside	-62.5%	-3.0%	2.3%	12.1%
	unburned	-2.6%	-2.9%	-97.3%	0.2%
Average		-18.7%	1.5%	-39.3%	5.3%

* Percent change could not be calculated for samples that began with no signal on day 0

Table 9: Model fit parameters for all Light-exposed samples

Component	Treatment	Intercept	Slope	R ²	p-value
Q1 (C11)	200°C	10.38	-0.10	0.97	0.000
	300°C	4.21	-0.53	0.80	0.016
	400°C	2.04	-0.49	0.96	0.001
	550°C	1.25	-0.37	0.97	0.000
	700°C	0.43	-0.13	0.97	0.000
	Outside	6.38	-0.68	0.76	0.024
	Unburned	12.10	-0.04	0.19	0.390
Q2 (C2)	200°C	18.18	-0.33	0.96	0.001
	300°C	8.18	-1.43	0.90	0.004
	400°C	3.97	-1.14	0.98	0.000
	550°C	2.13	-0.73	0.98	0.000
	700°C	0.82	-0.28	0.97	0.000
	Outside	11.03	-1.63	0.87	0.007
	Unburned	22.08	-0.25	0.87	0.007
Q3 (C12)	200°C	6.09	0.08	0.98	0.000
	300°C	9.47	-0.84	0.79	0.018
	400°C	5.35	-0.71	0.84	0.011
	550°C	3.14	-0.43	0.86	0.008
	700°C	0.55	-0.09	0.82	0.013
	Outside	10.71	-0.78	0.78	0.020
	Unburned	5.62	0.14	0.98	0.000
SQ1 (C5)	200°C	3.52	-0.12	0.70	0.039
	300°C	1.21	-0.29	1.00	0.000
	400°C	0.30	-0.11	0.99	0.000
	550°C	0.08	-0.03	0.96	0.001
	700°C	0.00	0.00	NaN	NaN
	Outside	1.39	-0.31	0.98	0.000
	Unburned	5.04	-0.15	0.79	0.018
SQ2 (C7)	200°C	2.966	-0.145	0.52	0.104
	300°C	1.307	-0.465	0.99	0.000
	400°C	0.372	-0.157	0.88	0.005
	550°C	0.029	0.005	0.54	0.097
	700°C	0.003	0.001	0.61	0.066

	Outside	1.488	-0.524	0.98	0.000
	Unburned	3.614	-0.155	0.70	0.038
SQ3 (C9)	200°C	-0.005	0.001	0.72	0.033
	300°C	2.415	-0.581	0.98	0.000
	400°C	1.334	-0.378	0.99	0.000
	550°C	0.390	-0.132	0.99	0.000
	700°C	0.144	-0.049	0.99	0.000
	Outside	1.924	-0.490	0.98	0.000
	Unburned	0.000	0.000	NaN	NaN
HQ (C4)	200°C	18.27	-0.44	0.89	0.005
	300°C	5.22	-1.12	0.97	0.000
	400°C	1.67	-0.59	0.96	0.000
	550°C	0.49	-0.13	0.74	0.027
	700°C	0.03	0.01	0.59	0.073
	Outside	7.31	-1.49	0.96	0.001
	Unburned	23.72	-0.46	0.92	0.003
Tryptophan (C8)	200°C	1.87	0.14	0.83	0.011
	300°C	4.03	-0.42	0.84	0.010
	400°C	2.35	-0.22	0.69	0.040
	550°C	0.95	0.00	0.00	0.968
	700°C	0.08	0.01	0.84	0.010
	Outside	4.48	-0.43	0.89	0.005
	Unburned	2.76	0.09	0.15	0.447
Tyrosine (C13)	200°C	3.460	-0.149	0.95	0.001
	300°C	2.460	-0.020	0.08	0.591
	400°C	0.830	0.002	0.00	0.926
	550°C	0.053	0.009	0.46	0.139
	700°C	0.002	0.000	0.02	0.787
	Outside	1.911	0.023	0.18	0.395
	Unburned	4.202	-0.171	0.97	0.000
**All 200°C and unburned treatments were fit to a linear model. All remaining treatments were fit to a logarithmic model.					
* n=6 for each treatment					

a. Quinone-like components (Q1, Q2, Q3)

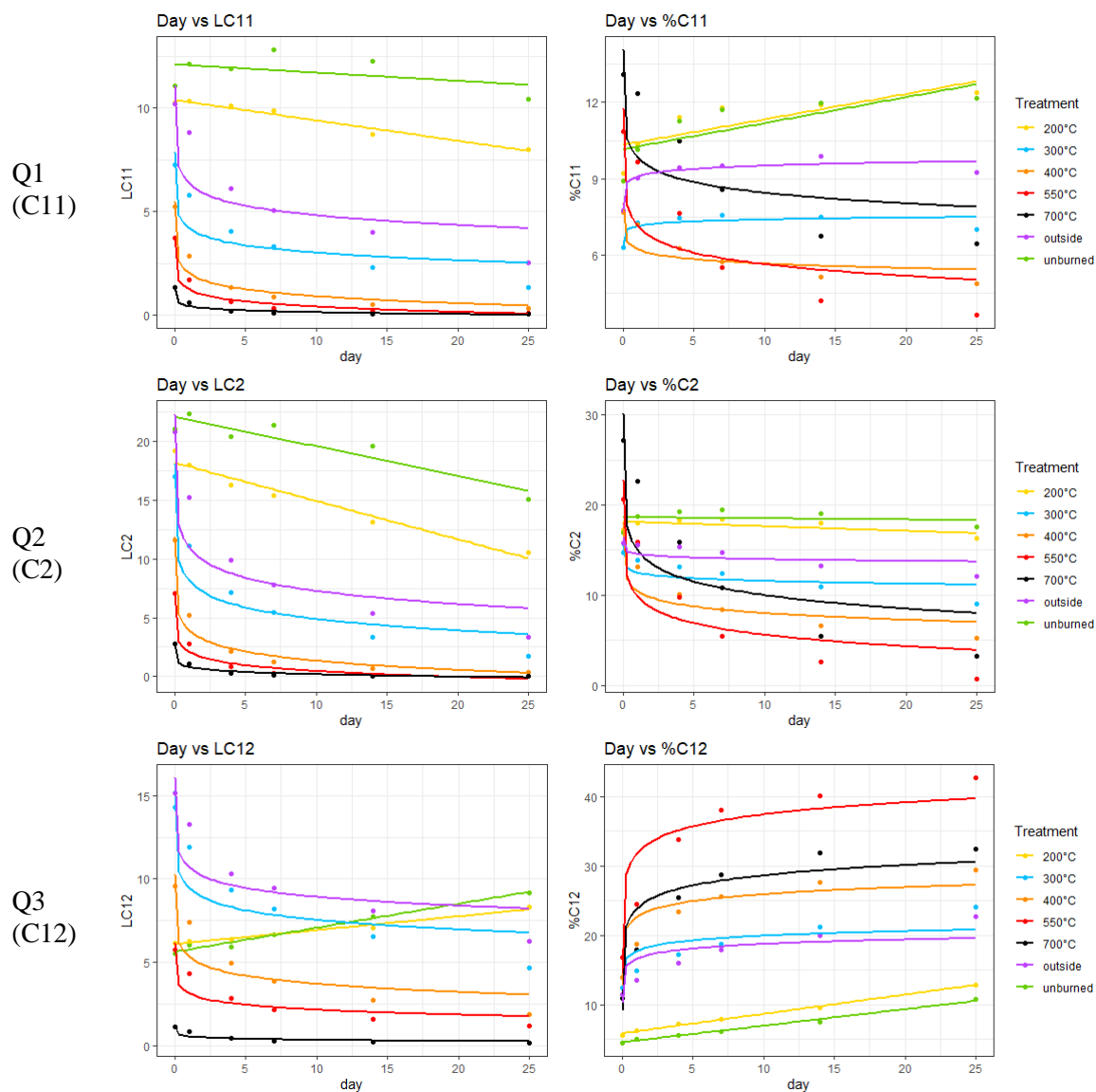


Figure 15: Absolute loading and percent loading of oxidized quinone-like (Q1, Q2, and Q3) components.

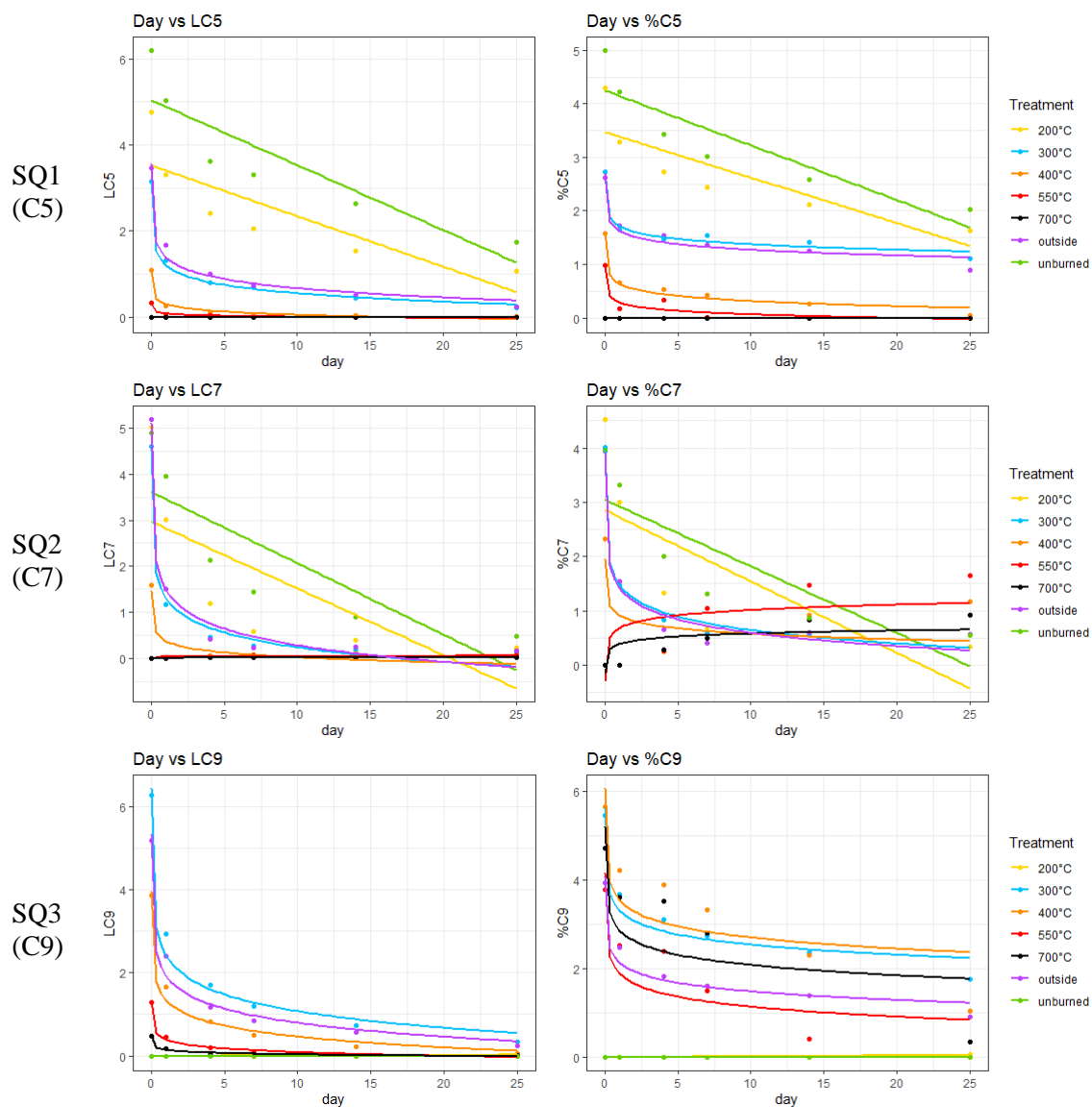
Quinone-like components (Q1, Q2, Q3) represent more oxidized quinone-like moieties. When examining the absolute loading of all quinone-like components (Q1, Q2, Q3), dark samples exhibit insignificant change over time, with the average percent change over the 25-day period being

7.9%, 4.7%, and 5% for Q1, Q2, and Q3, respectively (Table 8). Within this dark group, the higher temperature treatments (400, 550, and 700°C) exhibited a decrease in quinones whereas the lower temperature treatments (unburned, outside, 200, and 300°C) exhibited increases in quinones. Generally, the dark samples are not significantly changing.

The overall decrease in absolute loading correlates with an overall decrease in absorbance and overall decrease in total fluorescence. Almost all light-exposed samples exhibit a decrease in absolute loading with the average percent change over the 25-day exposure period being -67.5%, -77.6%, and -38.6% for Q1, Q2, and Q3, respectively (Table 8). Only the unburned and 200°C exhibited increases in Q3, 66% and 45% increases, respectively. The 200°C and unburned treatments were fit with a linear model with the following r-squared values: 0.97 (p-value < 0.001) and 0.19 (0.39 p-value) (Table 9). The remaining treatments (300, 400, 550, 700°C, and outside) were fit with a logarithmic model with the following r-squared values: 0.80 (p-value < 0.05), 0.96 (p-value= 0.001), 0.97 (p-value <0.001), 0.97 (p-value < 0.001), and 0.76 (p-value <0.05) (Table 9).

There is more variation in the percent loading for light-exposed samples, where all treatments experience a decrease in percentage of Q2, an increase in percentage of Q3, and a mixture of increasing (for lower temperature treatments) and decreasing (for higher temperature treatments) for Q1. This shows that photochemical transformation and potential cascading reactions involving radicals that may form larger compounds in the light-exposed samples, where both photodegraded and photoproducts may be forming within various treatments.

b. Reducing quinone-like components (SQ1, SQ2, SQ3, HQ)



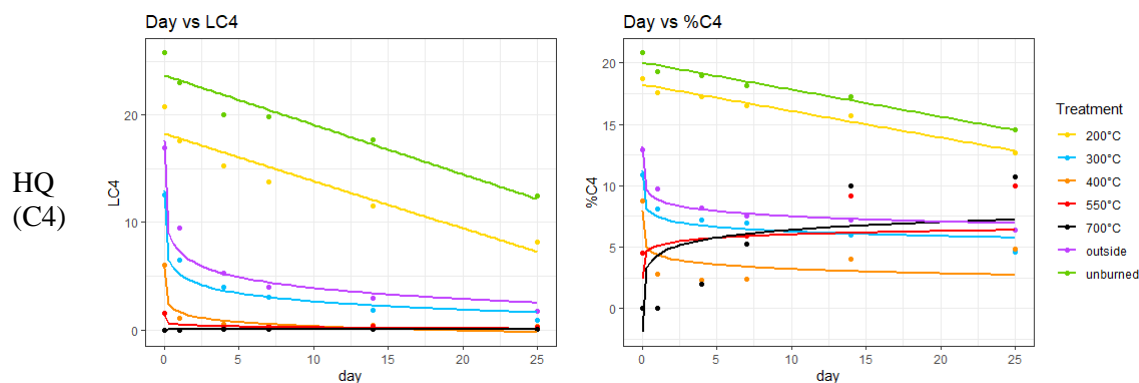


Figure 16: Absolute loading and percent loading of reduced quinone-like components, including semiquinone-like (SQ1, SQ2, and SQ3) and hydroquinone-like (HQ) component

Semiquinone-like (SQ1, SQ2, SQ3) and hydroquinone-like (HQ) components indicate more reduced DOM moieties (or red-shifted EEMs). Semiquinone-like species represent an intermediate quinone-like species and are therefore expected to be inherently lower percentages. When examining both the absolute loading and percent loading of all semi-quinone components (SQ1, SQ2, SQ3), most dark samples exhibit insignificant change over time (figure 16). However, within the dark-control group, the outside treatment exhibited the largest decrease in SQ2 and SQ3 compared to other treatments, which could potentially indicate that burn treatments involving atmospheric exposure and producing higher O:C ratios might be more susceptible to degrading with or without sunlight.

All light-exposed 700°C leachates exhibit no fluorescence signal for SQ1. All light-exposed unburned and 200°C leachates exhibit no fluorescence signal for SQ3. Within the remaining treatments, most light-exposed samples exhibit a decrease in absolute loading for semiquinone-like components. The 550 and 700°C exhibit insignificant change for all three semi-

quinone components. The unburned sample appears to experience a large decrease in SQ1 and SQ2.

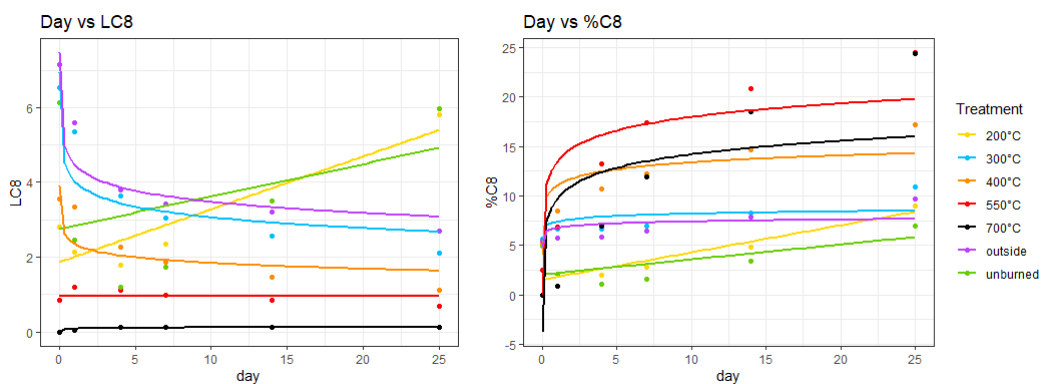
The percent loadings in SQ1 are similar in trend to the absolute loading, indicating there is a proportional decrease in the component compared to other components which can be attributed to an overall decline in absorbance. The 550 and 700°C treatments show an increase in percent loading of SQ2, while the absolute loadings exhibit only a slight increase indicating that despite the concentration of these components is not significantly changing the role of these reducing components is becoming inflated or more apparent as DOM photodegrades (ie. as other components decrease). This increase in SQ2 for the 550°C leachates and increase in HQ for the 700°C leachates could further support that DOM photolysis involves both the degradation and formation of species resulting from the formation of radical and reactive species.

The hydroquinone-like component represents the most reduced quinone-like fluorophore. When examining both the absolute loading and percent loading of HQ, most dark samples exhibit a slight decrease, but the change is insignificant over time. The light-exposed samples generally exhibit a more pronounced decrease in absolute loading. Except for the 550 and 700°C treatments, which show insignificant change in absolute loading but a significant increase in percentage loading, indicating that despite the concentration of these components is not significantly changing the role of these reducing components is becoming inflated or more apparent as DOM photodegrades (ie. as other components decrease). This shows that redox reactions and electron shuttling is occurring in the light-exposed samples, where both photodegraded and photoproducts may be forming within various treatments.

The changes in absolute loading of all these quinone-like components also underly the changes in the redox index (RI) values. The increase in RI for the 550 and 700°C leachates is associated with the large decrease in the oxidized components, Q1, Q2, and Q3, experiencing percent changes of -97.6%, -99.4%, and -85.4% for the 700°C leachates and -97.2%, -99.7%, and -80.3% for the 550°C leachates accompanied by slight increases in reducing components SQ2 and HQ for 700°C and SQ2 for 550°C (Table 8). The decrease in RI for the unburned and 200°C leachates is driven primarily by the complete loss of SQ3 coupled with the increase in Q3, 66.1% and 34.6% increase in Q3 for unburned and 200°C leachates respectively (Table 8).

c. Protein-like components (Tryptophan and Tyrosine)

Tryptophan
(C8)



Tyrosine
(C13)

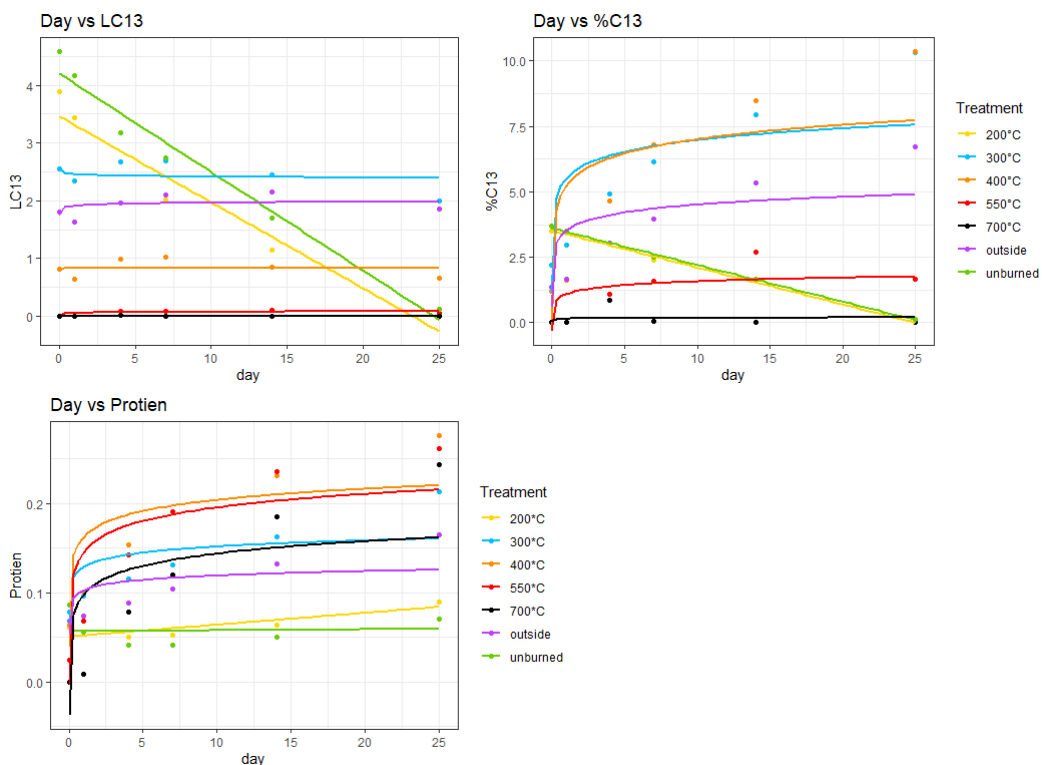


Figure 17: Absolute loading and percent loading of protein, amino acid-like components (tryptophan and tyrosine) and combined percent loadings of both tryptophan and tyrosine (Protein)

Figure 17 shows the absolute loading and percent loading of protein-like (tryptophan, tyrosine and combined) components. Dark control samples exhibited no significant change in protein composition (ie. the amino acid signals reflected in C8 and C13).

Light-exposed samples exhibited more variability in absolute loading. Most treatments showed a decrease in absolute loading for tryptophan, except for the 200°C and unburned treatments exhibited an increase. All treatments showed an increase in percent loading of tryptophan, with the larger increase observed in the higher treatment temperatures. This aligns with the previously observed blue-shifted EEMs. A previous study examining the role of nitrogen in marine CDOM found that out of several tested nitrogen compounds (including a compound containing tyrosine) only tryptophan contributed to the photochemical production of CDOM (Coble et al. 2014; Biers et al. 2007). The same study also found that tryptophan is prone to photosensitized oxidation, which could explain why the darker leachates (unburned and 200°C) experienced an increase in absolute loading of tryptophan since these darker solutions could have assisted in the absorption of solar radiation (Biers et al. 2007).

Most treatments showed an insignificant change in absolute loading for tyrosine, except for the 200°C and unburned treatments showing a decrease. Most treatments showed an increase in percent loading of tyrosine, again except for the 200°C and unburned showing a decrease. Overall, the light-exposed samples exhibited a greater increase in protein content proportional to other component signals, likely resulting from a decrease in the humic signal. The higher temperature samples were more susceptible to this change, from a proportional percent loading perspective. This could indicate that, in a natural system, the more labile and reactive compounds

found in the unburned and 200°C treatment could be consumed or photomineralized to CO₂. Whereas the higher temperature treatments are being partially oxidized into more labile LMW intermediate compounds which, in a natural system, could then be consumed by microbes.

The fact that protein content did not decrease provides reassurance that measures taken to prevent microbial influence (ie. formaldehyde, filtering, and autoclaving) were successful since typically protein content decreases during biotransformation (Cuss and Guéguen 2015).

SUMMARY

Overall, the production of hydrogen peroxide, the decrease in UV absorbance, and the observed shifts and decrease in fluorescence signatures indicated that the DPyOM was photochemically altered throughout the 25-day solar radiation exposure period. The decrease in CDOM and FDOM align with previous DOM photodegradation studies and represent an overall decrease in humic content (Cory McKnight 2007, Ward and Cory 2016; Hansen et al. 2016). Burn severity is an important factor influencing the fluorescence characteristics and trends of DPyOM. These results indicate that fluorescence spectroscopy could be useful in identifying DPyOM immediately post-wildfire or explaining temporal and downstream shifts.

Table 10 provides a summary of the fluorescence indices results and compares the photodegradation of DPyOM to the photodegradation of natural OM (NOM). DPyOM exhibits several similar fluorescence signatures that are within typical NOM ranges. Similar to NOM,

photodegraded DPyOM experiences a decrease in HIX and an increase in $\beta:\alpha$. Some differences unique to the thermally altered DPyOM include higher FI values, lower max EM_{370} , and lower RI values, especially DPyOM from higher burn temperatures. However, as these higher temperature DPyOM leachates experience prolonged exposure to solar radiation, the fluorescence signatures trend towards signatures that resemble NOM. While the magnitude of changes varied across burn treatments, the higher temperature leachates generally exhibited the largest overall change throughout the photodegradation experiment. Despite the level of thermal alteration, the direction of change was generally the same within a given index – except for the RI. The lower temperature leachates exhibited a decreasing RI, indicating a shift to more oxidized OM; whereas the higher temperature leachates exhibited an opposite increasing trend in RI, indicating that these photodegraded compounds are producing reducing reactive species.

Table 10: Summary values and trends of photodegraded DPyOM compared to photodegraded NOM

Index	DPyOM Experimental results	Comparison to NOM
HIX	<ul style="list-style-type: none"> • Values: within normal range; overall lower <ul style="list-style-type: none"> ○ Higher thermal alteration → much higher values to start 	→ Consistent with less mature or weathered NOM
	<ul style="list-style-type: none"> • Trend: Decreasing 	→ Typical for photodegraded NOM. Indicative of decreasing aromaticity or humification
$\beta:\alpha$	<ul style="list-style-type: none"> • Values: within normal range; overall slightly higher 	→ Consistent with typical NOM range (0.4-1)
	<ul style="list-style-type: none"> • Trend: Increasing 	→ Typical for photodegraded NOM
FI	<ul style="list-style-type: none"> • Values: mostly within range but overall lower <ul style="list-style-type: none"> ○ Higher thermal alteration → higher values 	→ Inconsistent for NOM. Elevated values likely due to shifted emission peak
	<ul style="list-style-type: none"> • Trend: Decreasing 	→ Photodegraded NOM typically does not experience significant changes
Max EM ₃₇₀	<ul style="list-style-type: none"> • Values: Higher thermal alteration → lower values 	→ Photodegraded NOM typically remains around 470nm
	<ul style="list-style-type: none"> • Trend: Increasing 	
RI	<ul style="list-style-type: none"> • Values: within normal range; overall slightly lower <ul style="list-style-type: none"> ○ Higher thermal alteration → lower values 	→ Consistent with NOM that is more oxidized.
	<ul style="list-style-type: none"> • Trend: Decreasing <ul style="list-style-type: none"> ○ Higher thermal alteration → Increasing values 	→ Photodegraded NOM has been shown to decrease slightly.

These results highlight that there are both photodegraded and photoproducts byproducts resulting from photoexposure and that the degree of thermal alteration of the parent material is important in assessing DPyOM dynamics. The shifting of the humic peak is consistent with previous DOM photochemical studies, representative of a decrease in aromaticity (or doubled bonded C) and with the production of reactive species. While the full range of potential reactive species were not identified within the scope of analyses performed in this study, the presence of H₂O₂ was quantified and is an indicator that reactive radical species were present (Beggs et al. 2009).

Highly concentrated leachates were intentionally generated in this experiment. In natural systems, the observed changes might occur at a faster rate due to less attenuation of UV light in the water column. Also, because wildfires produce a heterogeneous mixture of PyOM, natural systems will likely present a mixture of the chemical responses reported in this study. Furthermore, this study only examined the dissolved fraction, whereas a natural system will also include particulate OM that may be transported to an aquatic system. Future research should examine the coupling of both particulate and dissolved PyOM in addition to observing photochemical dynamics within a natural riverine system.

This study emphasizes that photodegradation is a significant degradation mechanism altering DPyOM. These results support an emerging and growing scientific viewpoint that indicate PyC can be quite mobile and reactive with turnover times of decades or years in soils rather than previously assumed millennia timescales. Photodegradation of DPyC could also explain the imbalance between PyC production and loss within the terrestrial landscapes and aquatic systems.

This enhanced reactivity and mobility coupled with the increasing occurrence and intensity of wildfires could have significant impacts on the global carbon budget. In addition, this increased PyC production and photodegradation could disrupt the energy balance of aquatic systems. Increasing wildfires will both increase the production of PyC but can also destroy canopies, leaving aquatic systems more vulnerable to UV penetration. Overall, DPyOM exhibits unique fluorescence signatures associated with varying degrees of thermal alteration. These unique signatures might become muted or merge with signatures similar to NOM with prolonged sun exposure, such as would occur in a lake or at higher order stream reaches with less riparian shading.

REFERENCES

- Abrajano, T. A., B. Yan, J. Song, R. Bopp, and V. O'Malley. 2007. "9.13 - High-Molecular-Weight Petrogenic and Pyrogenic Hydrocarbons in Aquatic Environments." In *Treatise on Geochemistry*, edited by Heinrich D. Holland and Karl K. Turekian, 1–50. Oxford: Pergamon. <https://doi.org/10.1016/B0-08-043751-6/09055-1>.
- Augustine, John A., John J. DeLuisi, and Charles N. Long. 2000. "SURFRAD—A National Surface Radiation Budget Network for Atmospheric Research." *Bulletin of the American Meteorological Society* 81 (10): 2341–58. [https://doi.org/10.1175/1520-0477\(2000\)081<2341:SANSRB>2.3.CO;2](https://doi.org/10.1175/1520-0477(2000)081<2341:SANSRB>2.3.CO;2).
- Beggs, Katherine M. H., R. Scott Summers, and Diane M. McKnight. 2009. "Characterizing Chlorine Oxidation of Dissolved Organic Matter and Disinfection By-Product Formation with Fluorescence Spectroscopy and Parallel Factor Analysis." *Journal of Geophysical Research: Biogeosciences* 114 (G4). <https://doi.org/10.1029/2009JG001009>.
- Biers, Erin J., Richard G. Zepp, and Mary Ann Moran. 2007. "The Role of Nitrogen in Chromophoric and Fluorescent Dissolved Organic Matter Formation." *Marine Chemistry* 103 (1): 46–60. <https://doi.org/10.1016/j.marchem.2006.06.003>.
- Bird, Michael I., Jonathan G. Wynn, Gustavo Saiz, Christopher M. Wurster, and Anna McBeath. 2015. "The Pyrogenic Carbon Cycle." *Annual Review of Earth and Planetary Sciences* 43 (1): 273–98. <https://doi.org/10.1146/annurev-earth-060614-105038>.
- Blank, Robert R., Fay L. Allen, and James A. Young. 1996. "Influence of Simulated Burning of Soil-Litter from Low Sagebrush, Squirreltail, Cheatgrass, and Medusahead on Water-Soluble Anions and Cations." *International Journal of Wildland Fire* 6 (3): 137–43.
- Blank, Robert R., Fay Allen, and James A. Young. 1994. "Extractable Anions in Soils Following Wildfire in a Sagebrush-Grass Community." *Soil Science Society of America Journal* 58 (2): 564–70. <https://doi.org/10.2136/sssaj1994.03615995005800020045x>.
- Bostick, Kyle W., Andrew R. Zimmerman, Andrew S. Wozniak, Siddhartha Mitra, and Patrick G. Hatcher. 2018. "Production and Composition of Pyrogenic Dissolved Organic Matter From a Logical Series of Laboratory-Generated Chars." *Frontiers in Earth Science* 6. <https://doi.org/10.3389/feart.2018.00043>.
- Brown, Roberta A., Andrew K. Kercher, Thanh H. Nguyen, Dennis C. Nagle, and William P. Ball. 2006. "Production and Characterization of Synthetic Wood Chars for Use as Surrogates for Natural Sorbents." *Organic Geochemistry* 37 (3): 321–33. <https://doi.org/10.1016/j.orggeochem.2005.10.008>.

- Cleveland, Cory C., Jason C. Neff, Alan R. Townsend, and Eran Hood. 2004. "Composition, Dynamics, and Fate of Leached Dissolved Organic Matter in Terrestrial Ecosystems: Results from a Decomposition Experiment." *Ecosystems* 7 (3): 175–285. <https://doi.org/10.1007/s10021-003-0236-7>.
- Coble, Paula G. 1996. "Characterization of Marine and Terrestrial DOM in Seawater Using Excitation-Emission Matrix Spectroscopy." *Marine Chemistry* 51 (4): 325–46. [https://doi.org/10.1016/0304-4203\(95\)00062-3](https://doi.org/10.1016/0304-4203(95)00062-3).
- Coble, Paula, Jamie Lead, Andy Baker, Darren M. Reynolds, and Robert G. Spencer, eds. 2014. *Aquatic Organic Matter Fluorescence*. Cambridge Environmental Chemistry Series. New York: Cambridge University Press.
- Cooper, William J., Rod G. Zika, Robert G. Petasne, and John M. C. Plane. 1988. "Photochemical Formation of Hydrogen Peroxide in Natural Waters Exposed to Sunlight." *Environmental Science & Technology* 22 (10): 1156–60. <https://doi.org/10.1021/es00175a004>.
- Coppola, Alysha I., Daniel B. Wiedemeier, Valier Galy, Negar Haghypour, Ulrich M. Hanke, Gabriela S. Nascimento, Muhammed Usman, et al. 2018. "Global-Scale Evidence for the Refractory Nature of Riverine Black Carbon." *Nature Geoscience* 11 (8): 584–88. <https://doi.org/10.1038/s41561-018-0159-8>.
- Cory, Rose M., and Diane M. McKnight. 2005. "Fluorescence Spectroscopy Reveals Ubiquitous Presence of Oxidized and Reduced Quinones in Dissolved Organic Matter." *Environmental Science & Technology* 39 (21): 8142–49. <https://doi.org/10.1021/es0506962>.
- Cory, Rose M., Diane M. McKnight, Yu-Ping Chin, Penney Miller, and Chris L. Jaros. 2007. "Chemical Characteristics of Fulvic Acids from Arctic Surface Waters: Microbial Contributions and Photochemical Transformations." *Journal of Geophysical Research: Biogeosciences* 112 (G4). <https://doi.org/10.1029/2006JG000343>.
- Cory, Rose M., Matthew P. Miller, Diane M. McKnight, Jennifer J. Guerard, and Penney L. Miller. 2010. "Effect of Instrument-Specific Response on the Analysis of Fulvic Acid Fluorescence Spectra." *Limnology and Oceanography: Methods* 8 (2): 67–78. <https://doi.org/10.4319/lom.2010.8.67>.
- Cotrufo, M. Francesca, Claudia M. Boot, Stephanie Kampf, Peter A. Nelson, Daniel J. Brogan, Tim Covino, Michelle L. Haddix, et al. 2016. "Redistribution of Pyrogenic Carbon from Hillslopes to Stream Corridors Following a Large Montane Wildfire." *Global Biogeochemical Cycles* 30 (9): 1348–55. <https://doi.org/10.1002/2016GB005467>.
- Cuss, C. W., and C. Guéguen. 2015. "Characterizing the Labile Fraction of Dissolved Organic Matter in Leaf Leachates: Methods, Indicators, Structure, and Complexity." In *Labile*

Organic Matter—Chemical Compositions, Function, and Significance in Soil and the Environment, 237–74. John Wiley & Sons, Ltd.
<https://doi.org/10.2136/sssaspecpub62.2014.0043>.

Del Vecchio, Rossana, and Neil V. Blough. 2004. “On the Origin of the Optical Properties of Humic Substances.” *Environmental Science & Technology* 38 (14): 3885–91.
<https://doi.org/10.1021/es049912h>.

Department of Atmospheric and Oceanic Sciences (ATOC). n.d. “Skywatch Observatory.” University of Colorado Boulder. <https://skywatch.colorado.edu/>.

Dittmar, Thorsten. 2008. “The Molecular Level Determination of Black Carbon in Marine Dissolved Organic Matter.” *Organic Geochemistry* 39 (4): 396–407.
<https://doi.org/10.1016/j.orggeochem.2008.01.015>.

Dittmar, Thorsten, Carlos Eduardo de Rezende, Marcus Manecki, Jutta Niggemann, Alvaro Ramon Coelho Ovalle, Aron Stubbins, and Marcelo Correa Bernardes. 2012. “Continuous Flux of Dissolved Black Carbon from a Vanished Tropical Forest Biome.” *Nature Geoscience* 5 (9): 618–22. <https://doi.org/10.1038/ngeo1541>.

“Doi:10.1016/j.Marchem.2005.04.003 | Elsevier Enhanced Reader.” n.d. Accessed June 17, 2020. <https://doi.org/10.1016/j.marchem.2005.04.003>.

Fellman, Jason B., Eran Hood, and Robert G. M. Spencer. 2010. “Fluorescence Spectroscopy Opens New Windows into Dissolved Organic Matter Dynamics in Freshwater Ecosystems: A Review.” *Limnology and Oceanography* 55 (6): 2452–62.
<https://doi.org/10.4319/lo.2010.55.6.2452>.

“Fluorescence Spectroscopy Reveals Ubiquitous Presence of Oxidized and Reduced Quinones in Dissolved Organic Matter | Environmental Science & Technology.” n.d. Accessed June 17, 2020. <https://pubs.acs.org/doi/10.1021/es0506962>.

Forbes, M. S., R. J. Raison, and J. O. Skjemstad. 2006. “Formation, Transformation and Transport of Black Carbon (Charcoal) in Terrestrial and Aquatic Ecosystems.” *Science of The Total Environment* 370 (1): 190–206. <https://doi.org/10.1016/j.scitotenv.2006.06.007>.

Gabor, Rachel S., Margaret A. Burns, Robert H. Lee, Jordan B. Elg, Cayla J. Kemper, Holly R. Barnard, and Diane M. McKnight. 2015. “Influence of Leaching Solution and Catchment Location on the Fluorescence of Water-Soluble Organic Matter.” *Environmental Science & Technology* 49 (7): 4425–32. <https://doi.org/10.1021/es504881t>.

Gao, Wei, John M. Davis, Roger Tree, James R. Slusser, and Daniel Schmoltdt. 2010. “An Ultraviolet Radiation Monitoring and Research Program for Agriculture.” In *UV Radiation in Global Climate Change: Measurements, Modeling and Effects on Ecosystems*, edited by

- Wei Gao, James R. Slusser, and Daniel L. Schmoldt, 205–43. Berlin, Heidelberg: Springer.
https://doi.org/10.1007/978-3-642-03313-1_8.
- Gunnarsson, Torsten, Peter Sundin, and Anders Tunlid. 1988. “Importance of Leaf Litter Fragmentation for Bacterial Growth.” *Oikos* 52 (3): 303–8.
<https://doi.org/10.2307/3565203>.
- Hader, Donat-P, Giulio Jori, A R Webb, P J Neale, David J Kieber, Robert G Wetzel, Mario Blumthaler, et al. 2003. *UV Effects in Aquatic Organisms and Ecosystems*. Edited by E Walter Helbling and Horacio Zagarese. Comprehensive Series in Photochemical & Photobiological Sciences. The Royal Society of Chemistry.
<https://doi.org/10.1039/9781847552266>.
- Hansen, Angela M., Tamara E. C. Kraus, Brian A. Pellerin, Jacob A. Fleck, Bryan D. Downing, and Brian A. Bergamaschi. 2016. “Optical Properties of Dissolved Organic Matter (DOM): Effects of Biological and Photolytic Degradation.” *Limnology and Oceanography* 61 (3): 1015–32. <https://doi.org/10.1002/lno.10270>.
- Hrncir, Duane C., and Diane McKnight. 1998. “Variation in Photoreactivity of Iron Hydroxides Taken from an Acidic Mountain Stream.” *Environmental Science & Technology* 32 (14): 2137–41. <https://doi.org/10.1021/es970986l>.
- Jaffé, R., J. N. Boyer, X. Lu, N. Maie, C. Yang, N. M. Scully, and S. Mock. 2004. “Source Characterization of Dissolved Organic Matter in a Subtropical Mangrove-Dominated Estuary by Fluorescence Analysis.” *Marine Chemistry* 84 (3): 195–210.
<https://doi.org/10.1016/j.marchem.2003.08.001>.
- Jaffé, Rudolf, Yan Ding, Jutta Niggemann, Anssi V. Vähätalo, Aron Stubbins, Robert G. M. Spencer, John Campbell, and Thorsten Dittmar. 2013. “Global Charcoal Mobilization from Soils via Dissolution and Riverine Transport to the Oceans.” *Science* 340 (6130): 345–47.
<https://doi.org/10.1126/science.1231476>.
- Jones, Matthew W., Cristina Santín, Guido R. van der Werf, and Stefan H. Doerr. 2019. “Global Fire Emissions Buffered by the Production of Pyrogenic Carbon.” *Nature Geoscience* 12 (9): 742–47. <https://doi.org/10.1038/s41561-019-0403-x>.
- Klapper, Lisa, Diane M. McKnight, J. Robin Fulton, Elizabeth L. Blunt-Harris, Kelly P. Nevin, Derek R. Lovley, and Patrick G. Hatcher. 2002. “Fulvic Acid Oxidation State Detection Using Fluorescence Spectroscopy.” *Environmental Science & Technology* 36 (14): 3170–75. <https://doi.org/10.1021/es0109702>.
- Kok, Gregory L., Kathleen. Thompson, Allan L. Lazrus, and Scott E. McLaren. 1986. “Derivatization Technique for the Determination of Peroxides in Precipitation.” *Analytical Chemistry* 58 (6): 1192–94. <https://doi.org/10.1021/ac00297a047>.

- Laane, R. W. P. M. 1982. "Influence of PH on the Fluorescence of Dissolved Organic Matter." *Marine Chemistry* 11 (4): 395–401. [https://doi.org/10.1016/0304-4203\(82\)90033-0](https://doi.org/10.1016/0304-4203(82)90033-0).
- Lazrus, Allan L., Gregory L. Kok, Sonia N. Gitlin, John A. Lind, and Scott E. McLaren. 1985. "Automated Fluorimetric Method for Hydrogen Peroxide in Atmospheric Precipitation." *Analytical Chemistry* 57 (4): 917–22. <https://doi.org/10.1021/ac00281a031>.
- Lei, Xia, Jiayi Pan, and Adam T. Devlin. 2019. "Characteristics of Absorption Spectra of Chromophoric Dissolved Organic Matter in the Pearl River Estuary in Spring." *Remote Sensing* 11 (13): 1533. <https://doi.org/10.3390/rs11131533>.
- Loh, Han Chern, Kok Wai Chong, and Musa Ahmad. 2007. "Quantitative Analysis of Formaldehyde Using UV-VIS Spectrophotometer Pattern Recognition and Artificial Neural Networks." *Analytical Letters* 40 (2): 281–93. <https://doi.org/10.1080/00032710600867606>.
- Macalady, Donald L., and Katherine Walton-Day. 2009. "New Light on a Dark Subject: On the Use of Fluorescence Data to Deduce Redox States of Natural Organic Matter (NOM)." *Aquatic Sciences* 71 (2): 135–43. <https://doi.org/10.1007/s00027-009-9174-6>.
- Masiello, C. A. 2004. "New Directions in Black Carbon Organic Geochemistry." *Marine Chemistry, New Approaches in Marine Organic Biogeochemistry: A Tribute to the Life and Science of John I. Hedges*, 92 (1): 201–13. <https://doi.org/10.1016/j.marchem.2004.06.043>.
- Masiello, C. A., and E. R. M. Druffel. 1998. "Black Carbon in Deep-Sea Sediments." *Science* 280 (5371): 1911–13. <https://doi.org/10.1126/science.280.5371.1911>.
- Masiello, C. A., and P. Louchouart. 2013. "Fire in the Ocean." *Science* 340 (6130): 287–88. <https://doi.org/10.1126/science.1237688>.
- Matosziuk, Lauren M., Adrian Gallo, Jeff Hatten, Kevin D. Bladon, Danica Ruud, Maggie Bowman, Jessica Egan, et al. 2020. "Short-Term Effects of Recent Fire on the Production and Translocation of Pyrogenic Carbon in Great Smoky Mountains National Park." *Frontiers in Forests and Global Change* 3. <https://doi.org/10.3389/ffgc.2020.00006>.
- McDowell, W. H., A. Zsolnay, J. A. Aitkenhead-Peterson, E. G. Gregorich, D. L. Jones, D. Jödemann, K. Kalbitz, B. Marschner, and D. Schwesig. 2006. "A Comparison of Methods to Determine the Biodegradable Dissolved Organic Carbon from Different Terrestrial Sources." *Soil Biology and Biochemistry* 38 (7): 1933–42. <https://doi.org/10.1016/j.soilbio.2005.12.018>.
- McDowell, William H., and Stuart G. Fisher. 1976. "Autumnal Processing of Dissolved Organic Matter in a Small Woodland Stream Ecosystem." *Ecology* 57 (3): 561–69. <https://doi.org/10.2307/1936440>.

- McKay, Garrett, and Fernando L. Rosario-Ortiz. 2015. "Temperature Dependence of the Photochemical Formation of Hydroxyl Radical from Dissolved Organic Matter." *Environmental Science & Technology* 49 (7): 4147–54. <https://doi.org/10.1021/acs.est.5b00102>.
- McKnight, Diane M., and George R. Aiken. 1998. "Sources and Age of Aquatic Humus." In *Aquatic Humic Substances: Ecology and Biogeochemistry*, edited by Dag O. Hessen and Lars J. Tranvik, 9–39. Ecological Studies. Berlin, Heidelberg: Springer. https://doi.org/10.1007/978-3-662-03736-2_2.
- McKnight, Diane M., Elizabeth W. Boyer, Paul K. Westerhoff, Peter T. Doran, Thomas Kulbe, and Dale T. Andersen. 2001. "Spectrofluorometric Characterization of Dissolved Organic Matter for Indication of Precursor Organic Material and Aromaticity." *Limnology and Oceanography* 46 (1): 38–48. <https://doi.org/10.4319/lo.2001.46.1.0038>.
- McKnight, Diane M., and Sabre M. Duren. 2004. "Biogeochemical Processes Controlling Midday Ferrous Iron Maxima in Stream Waters Affected by Acid Rock Drainage." *Applied Geochemistry*, A Tribute to Gunter Faure, 19 (7): 1075–84. <https://doi.org/10.1016/j.apgeochem.2004.01.007>.
- Miller, Matthew P., Diane M. McKnight, Rose M. Cory, Mark W. Williams, and Robert L. Runkel. 2006. "Hyporheic Exchange and Fulvic Acid Redox Reactions in an Alpine Stream/Wetland Ecosystem, Colorado Front Range." *Environmental Science & Technology* 40 (19): 5943–49. <https://doi.org/10.1021/es060635j>.
- Miller, Matthew P., Bailey E. Simone, Diane M. McKnight, Rose M. Cory, Mark W. Williams, and Elizabeth W. Boyer. 2010. "New Light on a Dark Subject: Comment." *Aquatic Sciences* 72 (3): 269–75. <https://doi.org/10.1007/s00027-010-0130-2>.
- Moran, Mary Ann, Wade M. Sheldon, and Richard G. Zepp. 2000. "Carbon Loss and Optical Property Changes during Long-Term Photochemical and Biological Degradation of Estuarine Dissolved Organic Matter." *Limnology and Oceanography* 45 (6): 1254–64. <https://doi.org/10.4319/lo.2000.45.6.1254>.
- Myers-Pigg, Allison N., Patrick Louchouart, and Roman Teisserenc. 2017. "Flux of Dissolved and Particulate Low-Temperature Pyrogenic Carbon from Two High-Latitude Rivers across the Spring Freshet Hydrograph." *Frontiers in Marine Science* 4. <https://doi.org/10.3389/fmars.2017.00038>.
- National Park Service (NPS). 2019. "Trees and Shrubs Checklist - Great Smoky Mountains National Park (U.S. National Park Service)." November 2019. <https://www.nps.gov/grsm/learn/nature/trees-shrubs-list.htm>.

- Novotny, Etelvino Henrique, Claudia Maria Branco de Freitas Maia, Márcia Thaís de Melo Carvalho, Beáta Emöke Madari, Etelvino Henrique Novotny, Claudia Maria Branco de Freitas Maia, Márcia Thaís de Melo Carvalho, and Beáta Emöke Madari. 2015. "BIOCHAR: PYROGENIC CARBON FOR AGRICULTURAL USE - A CRITICAL REVIEW." *Revista Brasileira de Ciência Do Solo* 39 (2): 321–44. <https://doi.org/10.1590/01000683rbc20140818>.
- Ohno, Tsutomu, Ivan J. Fernandez, Syuntaro Hiradate, and Jessica F. Sherman. 2007. "Effects of Soil Acidification and Forest Type on Water Soluble Soil Organic Matter Properties." *Geoderma* 140 (1): 176–87. <https://doi.org/10.1016/j.geoderma.2007.04.004>.
- Osburn, Christopher L., Thomas J. Boyd, Michael T. Montgomery, Thomas S. Bianchi, Richard B. Coffin, and Hans W. Paerl. 2016. "Optical Proxies for Terrestrial Dissolved Organic Matter in Estuaries and Coastal Waters." *Frontiers in Marine Science* 2. <https://doi.org/10.3389/fmars.2015.00127>.
- O'Sullivan, Daniel W., Patrick J. Neale, Richard B. Coffin, Thomas J. Boyd, and Christopher L. Osburn. 2005. "Photochemical Production of Hydrogen Peroxide and Methylhydroperoxide in Coastal Waters." *Marine Chemistry*, Special Issue in honor of Dana R. Kester, 97 (1): 14–33. <https://doi.org/10.1016/j.marchem.2005.04.003>.
- Otsuki, Akira, and Robert G. Wetzel. 1974. "Release of Dissolved Organic Matter by Autolysis of a Submersed Macrophyte, *Scirpus Subterminalis*1." *Limnology and Oceanography* 19 (5): 842–45. <https://doi.org/10.4319/lo.1974.19.5.0842>.
- Peacock, Mike, Chris D. Evans, Nathalie Fenner, Chris Freeman, Rachel Gough, Timothy G. Jones, and Inma Lebron. 2014. "UV-Visible Absorbance Spectroscopy as a Proxy for Peatland Dissolved Organic Carbon (DOC) Quantity and Quality: Considerations on Wavelength and Absorbance Degradation." *Environmental Science: Processes & Impacts* 16 (6): 1445–61. <https://doi.org/10.1039/C4EM00108G>.
- Petersen, Robert C., and Kenneth W. Cummins. 1974. "Leaf Processing in a Woodland Stream*." *Freshwater Biology* 4 (4): 343–68. <https://doi.org/10.1111/j.1365-2427.1974.tb00103.x>.
- Poulsen, James R., and John W. Birks. 1989. "Photoreduction Fluorescence Detection of Quinones in High-Performance Liquid Chromatography." *Analytical Chemistry* 61 (20): 2267–76. <https://doi.org/10.1021/ac00195a012>.
- Qualls, Robert G., Bruce L. Haines, and Wayne T. Swank. 1991. "Fluxes of Dissolved Organic Nutrients and Humic Substances in a Deciduous Forest." *Ecology* 72 (1): 254–66. <https://doi.org/10.2307/1938919>.

- Reisser, Moritz, Ross S. Purves, Michael W. I. Schmidt, and Samuel Abiven. 2016. "Pyrogenic Carbon in Soils: A Literature-Based Inventory and a Global Estimation of Its Content in Soil Organic Carbon and Stocks." *Frontiers in Earth Science* 4. <https://doi.org/10.3389/feart.2016.00080>.
- Santín, Cristina, Stefan H. Doerr, Agustin Merino, Thomas D. Bucheli, Rob Bryant, Philippa Ascough, Xiaodong Gao, and Caroline A. Masiello. 2017. "Carbon Sequestration Potential and Physicochemical Properties Differ between Wildfire Charcoals and Slow-Pyrolysis Biochars." *Scientific Reports* 7 (1): 11233. <https://doi.org/10.1038/s41598-017-10455-2>.
- Sasha Wagner. 2015. "Black Carbon: Sources, Mobility and Fate in Freshwater Systems." Dissertation, Florida International University.
- Schneider, Maximilian P. W., Michael Hilf, Ulrich F. Vogt, and Michael W. I. Schmidt. 2010. "The Benzene Polycarboxylic Acid (BPCA) Pattern of Wood Pyrolyzed between 200°C and 1000°C." *Organic Geochemistry* 41 (10): 1082–88. <https://doi.org/10.1016/j.orggeochem.2010.07.001>.
- Scott, Durelle T., Robert L. Runkel, Diane M. McKnight, Bettina M. Voelker, Briant A. Kimball, and Elizabeth R. Carraway. 2003. "Transport and Cycling of Iron and Hydrogen Peroxide in a Freshwater Stream: Influence of Organic Acids." *Water Resources Research* 39 (11). <https://doi.org/10.1029/2002WR001768>.
- Senesi, N., and V. D’Orazio. 2005. "FLUORESCENCE SPECTROSCOPY." In *Encyclopedia of Soils in the Environment*, edited by Daniel Hillel, 35–52. Oxford: Elsevier. <https://doi.org/10.1016/B0-12-348530-4/00211-3>.
- Soong, Jennifer L., William J. Parton, Francisco Calderon, Eleanor E. Campbell, and M. Francesca Cotrufo. 2015. "A New Conceptual Model on the Fate and Controls of Fresh and Pyrolyzed Plant Litter Decomposition." *Biogeochemistry* 124 (1): 27–44. <https://doi.org/10.1007/s10533-015-0079-2>.
- Steele, M. Kate, and Jacqueline A. Aitkenhead-Peterson. 2013. "Salt Impacts on Organic Carbon and Nitrogen Leaching from Senesced Vegetation." *Biogeochemistry* 112 (1): 245–59. <https://doi.org/10.1007/s10533-012-9722-3>.
- Stubbins, A., J. Niggemann, and T. Dittmar. 2012. "Photo-Lability of Deep Ocean Dissolved Black Carbon." *Biogeosciences* 9 (5): 1661–70. <https://doi.org/10.5194/bg-9-1661-2012>.
- Trevors, J. T. 1996. "Sterilization and Inhibition of Microbial Activity in Soil." *Journal of Microbiological Methods* 26 (1): 53–59. [https://doi.org/10.1016/0167-7012\(96\)00843-3](https://doi.org/10.1016/0167-7012(96)00843-3).

- Tuominen, Liisa, Timo Kairesalo, and Helinä Hartikainen. 1994. "Comparison of Methods for Inhibiting Bacterial Activity in Sediment." *Applied and Environmental Microbiology* 60 (9): 3454–57.
- United States Geological Survey (USGS). 2018. "Water Quality after a Wildfire." March 6, 2018. <https://ca.water.usgs.gov/wildfires/wildfires-water-quality.html>.
- Wagner, Sasha, Rudolf Jaffé, and Aron Stubbins. 2018. "Dissolved Black Carbon in Aquatic Ecosystems." *Limnology and Oceanography Letters* 3 (3): 168–85. <https://doi.org/10.1002/lol2.10076>.
- Ward, Collin P., and Rose M. Cory. 2016. "Complete and Partial Photo-Oxidation of Dissolved Organic Matter Draining Permafrost Soils." *Environmental Science & Technology* 50 (7): 3545–53. <https://doi.org/10.1021/acs.est.5b05354>.
- Wickland, Kimberly P., Jason C. Neff, and George R. Aiken. 2007. "Dissolved Organic Carbon in Alaskan Boreal Forest: Sources, Chemical Characteristics, and Biodegradability." *Ecosystems* 10 (8): 1323–40. <https://doi.org/10.1007/s10021-007-9101-4>.
- Wiedemeier, Daniel B., Susan Q. Lang, Merle Gierga, Samuel Abiven, Stefano M. Bernasconi, Gretchen L. Früh-Green, Irka Hajdas, et al. 2016. "Characterization, Quantification and Compound-Specific Isotopic Analysis of Pyrogenic Carbon Using Benzene Polycarboxylic Acids (BPCA)." *JoVE (Journal of Visualized Experiments)*, no. 111 (May): e53922. <https://doi.org/10.3791/53922>.
- World Health Organization. 2016. "Ultraviolet (UV) Radiation." March 2016. [https://www.who.int/news-room/q-a-detail/ultraviolet-\(uv\)-radiation](https://www.who.int/news-room/q-a-detail/ultraviolet-(uv)-radiation).
- Wymore, Adam S., Zacchaeus G. Compson, William H. McDowell, Jody D. Potter, Bruce A. Hungate, Thomas G. Whitham, and Jane C. Marks. 2015. "Leaf-Litter Leachate Is Distinct in Optical Properties and Bioavailability to Stream Heterotrophs." *Freshwater Science* 34 (3): 857–66. <https://doi.org/10.1086/682000>.

LIST OF ACRONYMS

DOC	Dissolved organic carbon
DOM	Dissolved organic matter
$\beta:\alpha$	Freshness Index
BPCA	benzene polycarboxylic acid. Molecular markers used to quantify PyC.
CDOM	Chromophoric DOM
CH ₂ O	Formaldehyde
DBC	Dissolved black carbon
DPyC	Dissolved PyC
FI	Fluorescence index
HCl	Hydrochloric acid
HIX	Humification index
HMW	high molecular weight
LMWOA	low molecular weight organic acids
NaHCO ₃	sodium bicarbonate
NOM	Natural organic matter
OM	Organic matter
PAHs	polycyclic aromatic hydrocarbons
PAR	Photosynthetically active radiation
PARAFAC	Parallel factor analysis
PPyC	Particulate PyC
PyC	Pyrogenic carbon
PyOM	Pyrogenic organic matter
RI	Redox index
TN	total nitrogen
UV	Ultraviolet
UV ₂₅₄	UV absorption at 254nm